

# Parametric model for capacity curves

Luis G. Pujades · Yeudy F. Vargas-Alzate ·  
Alex H. Barbat · José R. González-Drigo

The final publication is available at  
Springer via [http://  
dx.doi.org/10.1007/  
s10518-014-9670-5](http://dx.doi.org/10.1007/s10518-014-9670-5)

Received: 8 January 2014 / Accepted: 31 August 2014  
© Springer Science+Business Media Dordrecht 2014

**Abstract** A parametric model for capacity curves and capacity spectra is proposed. The capacity curve is considered to be composed of a linear part and a nonlinear part. The normalized nonlinear part is modelled by means of a cumulative lognormal function. Instead, the cumulative Beta function can be used. Moreover, this new conceptualization of the capacity curves allows defining stiffness and energy functions relative to the total energy loss and stiffness degradation at the ultimate capacity point. Based on these functions, a new damage index is proposed and it is shown that this index, obtained from nonlinear static analysis, is compatible with the Park and Ang index obtained from dynamic analysis. This capacity based damage index allows setting up a fragility model. Specific reinforced concrete buildings are used to illustrate the adequacy of the capacity, damage and fragility models. The usefulness of the models here proposed is highlighted showing how the parametric model is representative for a family of capacity curves having the same normalized nonlinear part and how important variables can be tabulated as empirical functions of the two main parameters defining the capacity model. The availability of this new mathematical model may be a powerful tool for current earthquake engineering research, especially in seismic risk assessments at regional scale and in probabilistic approaches where massive computations are needed.

**Keywords** Capacity curves · Parametric model · Stiffness degradation · Energy loss · Fragility curves · Damage assessment

## 1 Introduction

The capacity spectrum method, CSM (Freeman 1998a, b) is a fundamental tool for performance based design (PBD) (SEAOC 1995) and for estimating the expected seismic damage

L. G. Pujades (✉) · A. H. Barbat · J. R. González-Drigo  
Polytechnic University of Catalonia, BarcelonaTech, Jordi Girona 1-3, D2, 08034 Barcelona, Spain  
e-mail: lluis.pujades@upc.edu

Y. F. Vargas-Alzate  
Universidad Nacional de Colombia, Sede Manizales, Manizales, Colombia

in existing buildings. This method allows estimating, in a simplified and straightforward way, the displacement that a given earthquake, defined by its 5% damped response spectrum, would produce on a given building, defined by its capacity curve. Furthermore capacity spectra are used to define fragility curves allowing quantifying the expected seismic damage and risk. The capacity curve quantifies the strength of the building to lateral forces and represents the base shear as a function of the roof displacement. This curve is usually obtained from nonlinear static analysis, also known as *pushover* analysis. The response spectrum of a seismic action, defines the spectral acceleration as a function of the period. The acceleration-displacement format of the capacity curve is called capacity spectrum or capacity diagram (Chopra and Goel 1999). The inelastic response spectrum, also in the acceleration-displacement format is known as demand spectrum. Crossing capacity and demand spectra leads to an easy computation of the performance point which defines the spectral displacement that the earthquake will produce in the building. The relationships to calculate the capacity spectrum starting from the capacity curve and the procedures to obtain the performance point are well described in the report ATC-40 (ATC 1996). The spectral displacement of the performance point allows checking design requirements and expected performance levels. For damage assessment of existing buildings, this spectral displacement allows to evaluate the expected damage that the building would suffer when submitted to the earthquake. PBD has been well described by Sawyer (1964) and by Bertero (1996, 1997, 2000). Concerning to seismic risk assessment several approaches based on the CSM can be found in Pujades et al. (2012), Lantada et al. (2009), Barbat et al. (2008), Lagomarsino and Giovinazzi (2006) and FEMA (2002). Further developments and applications of the CSM can be found in Fajfar (1999), Chopra and Goel (1999), Fajfar and Gaspersic (1996) and Freeman et al. (1975). A review of the development of the CSM can be found in Freeman (2004). Figure 1 shows the capacity curve and the capacity spectrum of a seven stories reinforced concrete building. This building was analysed in detail by Vargas-Alzate et al. (2013a). An elastoplastic model was assumed to model the nonlinear behaviour of the materials in the pushover analysis. Table 1 shows the weights and normalized modal participation factors used to transform the capacity curve into the capacity spectrum. The bilinear form of the capacity spectrum is also shown in this figure. The bilinear capacity spectrum is widely used in the CSM (see for instance Freeman 1998a, b; ATC 1996) and is usually defined by two straight lines fulfilling the following conditions: (1) the first line is  $Sa = \omega^2 Sd$ , being  $Sa$  the spectral acceleration,  $Sd$  the spectral displacement and  $\omega$  the fundamental frequency of the building; for capacity curves, this line is  $F = K\delta$ , where  $F$  is the base shear,  $\delta$  is the roof displacement and  $K$  is the initial stiffness; (2) the

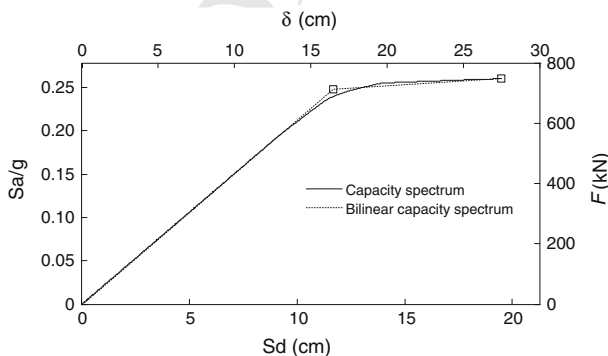


**Fig. 1** Capacity spectrum and capacity curve (*right and top axes*) for a seven storey reinforced concrete building. The bilinear form of the capacity spectrum is also shown

**Table 1** Weights,  $w_i$ , and normalized modal participation factors,  $\Phi_{i1}$  used to transform the capacity curve of Fig. 1 into the capacity spectrum

Storey	1	2	3	4	5	6	7
$w_i$ (kN)	485.16	527.23	479.47	518.76	501.93	553.27	471.65
$\Phi_{i1}$	0.14	0.30	0.45	0.60	0.67	0.85	1.00

second line goes through the ultimate capacity point and (3) the areas below the capacity spectrum and the bilinear capacity form are the same (energy condition). So, this bilinear capacity spectrum is defined by the effective yielding point,  $(D_y, A_y) = (11.7 \text{ cm}, 0.25 \text{ g})$ , and the effective inelastic limit or ultimate capacity point,  $(D_u, A_u) = (19.5 \text{ cm}, 0.26 \text{ g})$ . These two points are well described in Freeman (1998a). Conditions 2 and 3 must be fulfilled in any case. Sometimes, as for instance when an elastoplastic model is assumed for the bilinear capacity spectrum, the slope of the first branch of the bilinear capacity spectrum can be lower than the one corresponding to the fundamental period of the building.

The ultimate capacity point was initially defined (Freeman 2004) as the base shear causing the most flexible lateral force resisting elements to yield after the more rigid elements yielded or failed and it is usually defined by the displacement for which a collapse mechanism has been produced so that the strength of the structure has been exhausted. This paper proposes a model that re-conceptualizes capacity curves in the context of the CSM. The core of the model lies into the separation of the linear and nonlinear behaviors of the structures when submitted to lateral loads. It is explicitly shown that the normalized nonlinear part fully represents the degradation of the building from sound to collapse states for a family of structures and that this can be represented by only two parameters. Based on this reconceptualization, a new damage model is then proposed. The damage model allows separating the contributions to damage of stiffness degradation and that of energy loss resulting in a new damage index. This index is analyzed and compared with other indices widely used for seismic damage and risk assessment. Finally several of the advantages of the models in the current earthquake engineering practice are highlighted and discussed.

## 2 Capacity model

This section is devoted to describe the parametric model for capacity curves. In a first step the capacity curve is analysed and separated into two functions, linear and nonlinear, composing the true capacity curve. The derivatives of these two functions are also fundamental for the formulation of the model. Afterwards the model itself is formulated and, finally, it is shown how the true capacity curve can be reconstructed from five parameters.

### 2.1 Anatomy of the capacity curve

Capacity curves can be considered composed of a linear part and a nonlinear part. The linear part would be the capacity curve assuming that the building has a linear and elastic behaviour and it is represented by a straight line whose slope is defined by the period of the fundamental mode of vibration of the structure. The nonlinear part would contain strictly the nonlinear response of the building and can be obtained by subtracting the true capacity curve from the linear curve. Thus, the nonlinear part,  $F_{NL}(\delta)$ , can be obtained by means of the following equation:

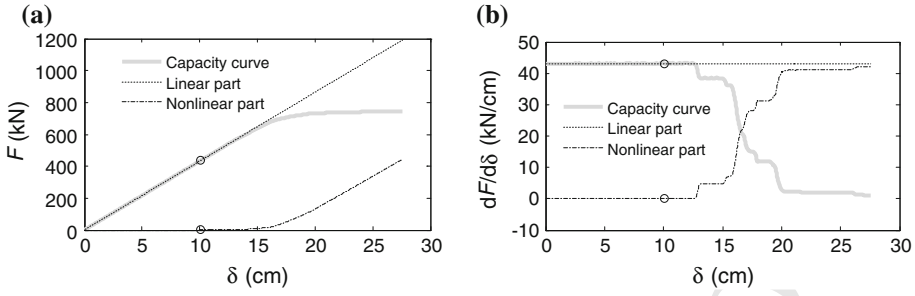


**Fig. 2** **a** Capacity curve and its linear and nonlinear parts. **b** First derivatives of the capacity curve and of its linear and nonlinear parts

$$F_{NL}(\delta) = F_L(\delta) - F(\delta) = m \delta - F(\delta) \tag{1}$$

where  $\delta$  is the roof displacement,  $F(\delta)$  is the true pushover curve and  $F_L(\delta) = m \delta$  is linear part being  $m$  the slope of the first leg of the capacity curve that is linked to the fundamental period of the building. Figure 2a shows the capacity curve  $F(\delta)$  of Fig. 1 and its linear and nonlinear parts; Fig. 2b shows the corresponding derivatives:  $dF(\delta)/d\delta$ ,  $dF_{NL}(\delta)/d\delta$  and  $dF_L(\delta)/d\delta = m$ .

In this case  $m$  is 43.15 kN/cm and circle markers indicate the beginning of the nonlinear behaviour of the structure. The value of the displacement at this point is  $\delta = 10.1$  cm. From Eq. (1) it follows that the function  $dF_{NL}(\delta)/d\delta$  fulfils the following equation:

$$\frac{d}{d\delta} F_{NL}(\delta) = m - \frac{d}{d\delta} F(\delta) \tag{2}$$

The first derivative of the capacity curve and indeed that one of the nonlinear part, (see Fig. 2b) allow observing the progressive degradation of the structure. The model here proposed is based on the fit of the normalized nonlinear part of the capacity curve and, therefore, the same model is valid for both capacity curves and capacity spectra. Another advantage of the model lies in its ability to simultaneously fitting both the capacity curve and their first and second derivatives. The derivatives are related to the tangent stiffness and to the progressive degradation of the strength of the structure.

### 2.2 Parameters of the capacity model

The first step to fit a parametric model is the normalization of the nonlinear part of the capacity curve and its first derivative. The model assumes that the normalized first derivative of the nonlinear part is well represented by a cumulative lognormal function as defined in Eqs. (4) and (5). That is, the scaled first derivative,  $\Psi'$ , and the derivative of this,  $\Psi''$ , satisfy the following equations:

$$\Psi'(A\delta) = B \frac{dF_{NL}(\delta)}{d\delta} \quad 0 \leq A\delta \leq 1 \tag{3}$$

$$\Psi''(A\delta) = \frac{1}{(A\delta) \sigma \sqrt{2\pi}} e^{\frac{-(\ln(A\delta) - \ln(\mu))^2}{2\sigma^2}} \quad 0 \leq A\delta \leq 1 \tag{4}$$

$$\Psi'(A\delta) = \int_0^{A\delta} \Psi''(\xi) d(\xi) \quad 0 \leq A\delta \leq 1 \tag{5}$$

Author Proof

$$F_{NL}(A\delta) = \frac{1}{B} \int_0^{A\delta} \Psi'(\xi) d\xi, \quad 0 \leq A\delta \leq 1 \tag{6}$$

*A* and *B*, are scaling constants. The following equation defines these constants.

$$A = 1/\delta_{max} \quad \text{and} \quad \frac{1}{B} = \frac{1}{m - m^*} \tag{7}$$

Where *m* is the slope at the beginning of the capacity curve, or equivalently, the slope of the linear part of the capacity curve and *m\** is the slope at the end of the capacity curve. Observe that *m* and *m\** also are respectively the maximum and minimum values of the first derivative of the capacity curve (grey colour curve in Fig. 2b); *m* = 43.19 kN/cm, *m\** = 1.12kN/cm, *A* = 27.54 cm and *B* = 42.07 kN/cm in this case. Thus, the scaled first derivative is defined for normalized displacements,  $\delta_N = A\delta$ , taking values between zero and one and ranging also between zero and one the values of this function.  $\Psi''(A\delta)$  is the standard lognormal distribution function defined by the parameters  $\mu$  and  $\sigma$ . A least squares fit between the target and computed,  $F_{NL}(A\delta)$ , functions allows to determine the two parameters of the model. Instead of the lognormal function, the cumulative Beta function can be used. In this case, Eq. (4) is substituted by the following equation:

$$\Psi''(x) = \frac{1}{B(\lambda, \nu)} x^{\lambda-1} (1-x)^{\nu-1} \quad 0 \leq x \leq 1 \quad (x = A\delta) \tag{8}$$

being  $B(\lambda, \nu) = \int_0^1 t^{\lambda-1} (1-t)^{\nu-1} dt = \frac{\Gamma(\lambda)\Gamma(\nu)}{\Gamma(\lambda+\nu)}$  and  $\Gamma(\alpha) = \int_0^\infty e^{-t} t^{\alpha-1} dt$ .

For random variables defined by a lognormal probability density function as defined in Eq. (4), or with a Beta probability density function as defined in Eq. (8), the mean,  $M_L$ , and variance  $V_L$ , or  $M_B$  and  $V_B$  respectively, are functions of the parameters of the lognormal distribution ( $\mu, \sigma$ ) or of the Beta distribution ( $\lambda, \nu$ ). To avoid confusion with other more standard definitions of the lognormal distribution, where the first parameter of the distribution is defined as  $\mu' = \ln(\mu)$  (see for instance Limpert et al. 2001), the equations used to infer mean and variance values are reproduced herein.

$$M_L = e^{\left(\ln\mu + \frac{\sigma^2}{2}\right)}, \quad V_L = e^{(2\ln\mu + \sigma^2)} \left(e^{\sigma^2} - 1\right) \quad \text{and} \quad M_B = \frac{\lambda}{\lambda + \nu},$$

$$V_B = \frac{\lambda\nu}{(\lambda + \nu + 1)(\lambda + \nu)^2} \tag{9}$$

The model of Eq. (4), with  $\ln(\mu)$  instead of  $\mu'$ , has been preferred because now  $\mu$  is close to  $M_L$  and can be estimated approximately from the normalized first derivative of the non-linear part of the capacity curve, thus allowing constraining the variability of the  $\mu$  parameter in the search by the least squares fit procedure. The same election was taken in the Risk-UE project to model fragility curves (Milutinovic and Trendafiloski 2003). Moreover, as it can be seen in Table 2, this choice also leads to comparable mean values and variances of the fitted lognormal and Beta distributions. Table 2 shows the parameters of the fit.

In this table  $\mu$  and  $\sigma$  are the parameters of the lognormal function as defined in Eq. (4);  $\lambda$  and  $\nu$  are the parameters defining the Beta function.  $M_L$  and  $V_L$ , and  $M_B$  and  $V_B$  are the mean values and variances of the distribution functions, for the lognormal and Beta cases respectively. Figure 3 summarizes the results of the fit. The capacity curve, the linear part and the nonlinear part, together with their first and second derivatives, are shown.

Author Proof

**Table 2** Parameters of the models fitting the capacity curve of Fig. 2

Lognormal				Beta			
$\mu$	$\sigma$	Mean ( $M_L$ )	Variance ( $V_L$ )	$\lambda$	$\nu$	Mean ( $M_B$ )	Variance ( $V_B$ )
0.608	0.12	0.6124	0.0054	21.10	13.07	0.618	0.007

The corresponding mean values and variances are also shown

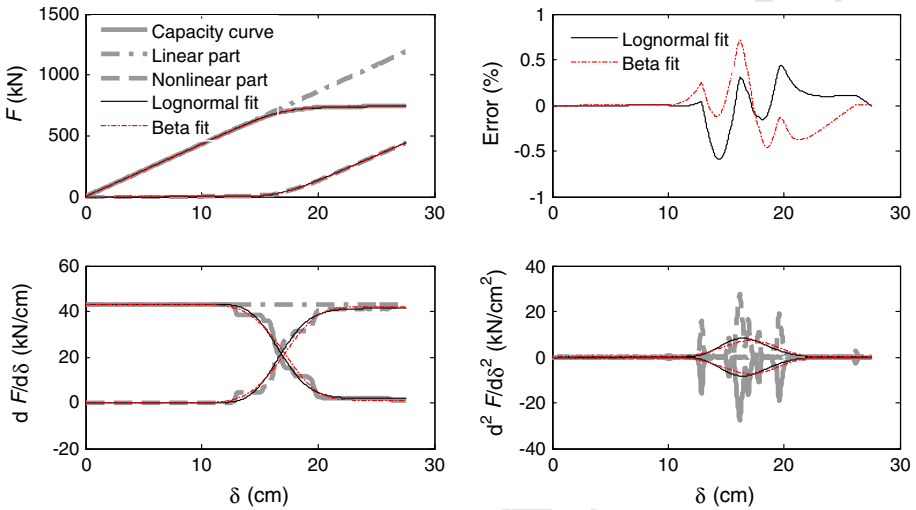


**Fig. 3** Capacity curve, linear and nonlinear parts (*top left*). First (*bottom left*) and second (*bottom right*) derivatives. Target and fitted curves are shown for lognormal and Beta models. *Top right plot* shows the differences, in %, between target and fitted capacity curves

156 The differences between the observed and fitted capacity curves are also shown (top  
 157 right). The differences are very small and always below 1 %. The mean value,  $d_m$ , and the  
 158 standard deviation,  $d_{std}$ , of the vector of differences, for the lognormal, L, and Beta, B,  
 159 cases respectively, are:  $d_{mL} = 0.013 \%$ ,  $d_{stdL} = 0.18$  and  $d_{mB} = -0.04 \%$ ,  $d_{stdB} = 0.21$ .  
 160 The parametric model has been tested with a significant number of capacity curves and  
 161 capacity spectra, with excellent results in all the cases. The errors have been comparable  
 162 to those obtained in the example presented here. Similar results are obtained when using  
 163 lognormal and Beta functions. So, either of the two can be used. Probably these adequate  
 164 fits are due to the fact that the model matches well the physical processes involved in the  
 165 structural degradation. In this article the lognormal function has been preferred because it is  
 166 widely used in many problems in earthquake engineering (ATC 1985, 1991; FEMA 2002;  
 167 Lagomarsino and Giovinazzi 2006; Barbat et al. 2008; Pujades et al. 2012) and because the  
 168 interpretation of the model parameters is more direct. However, the fact that the lognormal  
 169 function has an asymptotic trend, while the non-linear part of the capacity curve is limited  
 170 to  $\delta_{max}$  and normalized at this point, the Beta function would be more appropriate because  
 171 it is defined in the limited domain.

172 *Summary of the fitting procedure*

173 The steps followed for the adjustment of the capacity curve of Fig. 3 are summarized here.  
 174 (i) The first derivative of the capacity curve is calculated and the slope,  $m = 43.15 \text{ kN/cm}$ ,  
 175 that defines the linear part of the capacity curve is inferred. Considering that in the linear

Author Proof

part of the capacity spectrum,  $Sa = \omega^2 Sd = m_{cs} Sd$ , being  $\omega$  the angular frequency of the fundamental mode of vibration of the building, the slope  $m_{cs}$  of the linear part of the capacity spectrum, can be also obtained from the fundamental period of the building, assuming that the proper units are used, for instance,  $\text{cm/s}^2$  and  $\text{cm}$  respectively for  $Sa$  and  $Sd$ ;  $m_{cs} = 20.96 \text{ s}^{-2}$  in this case. When the capacity curve is used, the factors converting the capacity curve to capacity spectrum allow calculating  $m$  from  $m_{cs}$ . (ii) The nonlinear part of the capacity curve is obtained (see Eq. (1), Fig. 2). (iii) Abscissae and ordinates are scaled dividing by their maximum values, which in this case are 27.54 cm for abscissae and 441.61 kN for ordinates. (iv) Optionally, the derivative of the nonlinear part of the capacity curve (see Fig. 3) can be also calculated and normalized; in fact, this step gives an idea of the approximate parameters of the lognormal function of the parametric model, thus allowing constraining the search range of the parameters. (v) For each pair of parameters,  $(\mu, \sigma)$ , the function defined in Eq. (6) is obtained by using Eq. (4); this function is also normalized on abscissae and ordinates; a least squares fit between the curve so calculated and the curve found in step iii), provides the best parameter pair of the fit. In the example of Fig. 3,  $\mu$  has been varied between 0.46 and 0.72, with a resolution of 0.005 units and  $\sigma$  between 0.01 and 2, with a resolution value of 0.01; the final values of the fits are shown in Table 2. (vi) Equations (1–6) allow the reconstruction of all the functions involved, simply undoing the normalizations made. Figure 3 shows the results of the implementation of these 6 steps. The results using Lognormal and Beta functions are displayed. The differences between the target curve and the parametric curve are also shown in this figure, giving a precise idea of the goodness of the fits. An additional advantage of the model is its ability to represent well not only the target curve but also its successive derivatives. Taking into account that a simple scaling allows converting capacity curves into capacity spectra and, given the normalizations involved in the fitting method, it is important to outline that the same model holds for capacity curves and capacity spectra. As the case presented here shows a clearly defined linear portion, yielding point and hardening slope, a capacity curve showing neither clear linear portion nor yielding point and exhibiting negative stiffness (softening) after the post-peak response will be analyzed below.

### 2.3 Synthesis of the capacity spectrum

In addition to  $\mu$  and  $\sigma$ , capacity spectra also depend on the following parameters: (1) the slope  $m$  of the linear part; (2) the ultimate spectral displacement,  $Sd_u$ ; and (3) the spectral acceleration,  $Sa_u$ , of the ultimate capacity point. Therefore, a capacity curve is entirely defined by the following five independent parameters:  $\mu, \sigma, m, Sd_u$  and  $Sa_u$ . Consequently, families of capacity spectra have the same lognormal or Beta model. The construction of these curves is simple and straightforward undoing the steps explained above (see Eqs. 3–8). Figure 4 shows an example of reconstruction of a capacity spectrum from these 5 parameters. The numerical values of the parameters are also shown in this figure. As pointed out above, the initial stiffness  $m$  and the fundamental period of the building are directly related. Therefore it may be more intuitive to use the fundamental period, instead than  $m$ , as one of the five independent parameters.

## 3 Damage model

In this section a new damage model is proposed. The model is based on stiffness degradation and energy dissipation relative to the residual stiffness and total energy at the ultimate capacity point.

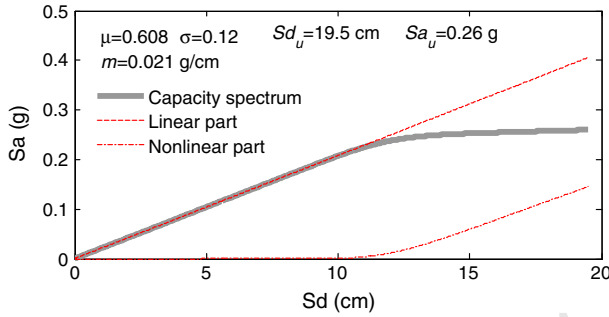


Fig. 4 Capacity spectrum defined by five independent parameters

220 A reinforced concrete building is used to illustrate the practical computation of the model.  
 221 Incremental dynamic analysis is performed to obtain the Park and Ang (1985) damage index.  
 222 Then, the new damage index is calculated and calibrated so that it is equivalent to the Park  
 223 and Ang index. This new damage index is obtained from the capacity curve by means of  
 224 simple and straightforward calculations.

225 3.1 Definition of the new damage index

226 Cosenza and Manfredi (2000) review the ground motion parameters that, directly or indirectly,  
 227 can be linked to structural and non-structural damage. They consider parameters related to the  
 228 acceleration time histories, to the response spectra and to the step-by-step dynamic analysis.  
 229 Park and Ang (1985) propose an index to assess the expected structural seismic damage in  
 230 reinforced concrete buildings (see also Park 1984). Buildings are weakened and damaged due  
 231 to two combined effects: (1) large displacements caused by their response to large stresses  
 232 and (2) cyclic drifts in response to cyclic strains. Consequently, Park and Ang claim that  
 233 the assessment of damage must consider not only the maximum structural response but also  
 234 repeated cyclic loads typical of seismic actions, mainly depending on their duration. The  
 235 Park and Ang index is widely used and it can be defined by Eq. (10) or, equivalently, by  
 236 Eq. (11).

$$237 DI_{PA}(\delta) = \frac{\delta}{\delta_u} + \frac{\beta}{Q_y \delta_u} \int_0^\delta dE \tag{10}$$

$$238 DI_{PA}(\delta) = \frac{\delta}{\delta_u} + \beta \int_{\xi=0}^\delta \left( \frac{\xi}{\delta_u} \right)^\alpha \frac{dE}{Ec(\xi)} \tag{11}$$

239  $\delta$  is the maximum deformation of the building under the earthquake motion,  $\delta_u$  is the ultimate  
 240 deformation under monotonic loads and  $Q_y$  is the strength at the yielding point. If the strength,  
 241  $Q_u$ , at the ultimate point,  $\delta_u$ , is lower than  $Q_y$ , then  $Q_y$  is substituted by  $Q_u$ .  $Ec(\xi)$  is the  
 242 hysteretic energy dissipated in each cycle of load at the deformation  $\xi$ ,  $dE$  is the incremental  
 243 hysteretic energy absorbed;  $\alpha$  and  $\beta$  are non-negative parameters.

244 In the elastic response range, theoretically, the value of  $DI_{PA}$  is null, but its effective  
 245 calculus through Eqs. (10) or (11) may result in positive negligible values.  $DI_{PA} \geq 1$  implies  
 246 total damage or collapse. Thus, the structural damage is a function of the deformation and  
 247 of the energy dissipated. Both quantities depend on the load history, while the parameters  $\alpha$ ,



248  $\beta$ ,  $\delta_u$ ,  $Q_u$  and  $E_c(\xi)$  are independent of the load history. Equation (11) takes into account  
 249 the effects of cyclic loads at different levels of deformation, while in Eq. (10) it is assumed  
 250 that this effect is uniform and the same at all deformations. So,  $DI_{PA}$  can be defined by a  
 251 linear combination of the maximum displacement of response and dissipated energy. Indeed,  
 252 Williamson and Kaewkulchai (2004) define  $DI_{PA}$ , in a simplified way, by means of the  
 253 following equation:

$$DI_{PA}(\delta) = \alpha U(\delta) + \beta W(\delta) \tag{12}$$

255  $\alpha$  and  $\beta$  are constants,  $U(\delta)$  is a function that depends on the maximum deformation reached  
 256 and  $W(\delta)$  is a function that depends on the energy dissipated.  $\alpha$  and  $\beta$  can be adjusted to  
 257 take into account different ratios of damage accumulation, thus representing a wide variety  
 258 of response models proposed in the literature (Williamson 2003).

259 Coming back to the capacity curve, we have seen how the information of the structural  
 260 degradation is in its nonlinear part. In relative terms, that is, as a fraction of the total degrada-  
 261 tion in the ultimate deformation, this information is also well represented by two functions  
 262 that depend only on the nonlinear part of the capacity curve, once abscissae and ordinates have  
 263 been normalized. These two functions are defined next. Let's call  $E(\delta)$  and  $K(\delta)$  functions  
 264 respectively related to energy dissipation and stiffness degradation.

265  $E(\delta)$  is easily obtained from the integration of the nonlinear part of the capacity curve;  
 266 that is:

$$E(\delta) = \int_0^\delta F_{NL}(\xi)d\xi; \quad 0 \leq \delta \leq \delta_u; \quad 0 \leq E(\delta) \leq E(\delta_u) \tag{13}$$

268  $F_{NL}(\xi)$  is the nonlinear part of the capacity curve and has dimensions of force;  $\delta$  and  $\xi$  are  
 269 displacements; thus,  $E(\delta)$  has dimensions of energy and is related to the energy dissipated  
 270 by the structure when it reaches a displacement  $\delta$ . It is worth noting that even though  $E(\delta)$   
 271 has dimensions of energy, it is not directly related to the cyclic hysteretic dissipation, as it  
 272 is implicit in the Park and Ang index as defined in Eqs. (10–12). We will see that it is more  
 273 general and useful to work with the function normalized in abscissae and in ordinates. The  
 274 following equation defines this normalized function  $E_N(\delta_N)$ :

$$E_N(\delta_N) = \frac{E(\delta/\delta_u)}{E(\delta_u)}; \quad 0 \leq \delta_N \leq 1; \quad 0 \leq E_N(\delta_N) \leq 1; \tag{14}$$

276  $E_N(\delta_N)$  is the ratio between the energy dissipated as a function of the relative displacement,  
 277  $\delta_N = \delta/\delta_u$ , and the total energy that the structure has dissipated at the ultimate displacement  
 278  $E(\delta_u)$ .

279 The second function is related to stiffness and is defined by the following equation:

$$K(\delta) = \frac{F(\delta)}{\delta} \tag{15}$$

281  $K(\delta)$  also can be transformed into another one varying between 0 and 1 and depending only  
 282 on the nonlinear part. Actually, considering that the linear part is defined as  $F_L(\delta) = m\delta$  and  
 283 that  $F(\delta) = F_L(\delta) - F_{NL}(\delta)$  it can be shown that:

$$\overline{\overline{K_{NL}(\delta)}} = \frac{\left[ \frac{F_{NL}(\delta)}{\delta} \right]_{\max} - \frac{F_{NL}(\delta)}{\delta}}{\left[ \frac{F_{NL}(\delta)}{\delta} \right]_{\max} - \left[ \frac{F_{NL}(\delta)}{\delta} \right]_{\min}} = \frac{\left[ \frac{F(\delta)}{\delta} \right]_{\max} - \frac{F(\delta)}{\delta}}{\left[ \frac{F(\delta)}{\delta} \right]_{\max} - \left[ \frac{F(\delta)}{\delta} \right]_{\min}}; \tag{16}$$

$$0 \leq \overline{\overline{K_{NL}}} \leq 1; \quad 0 \leq \delta \leq \delta_u$$

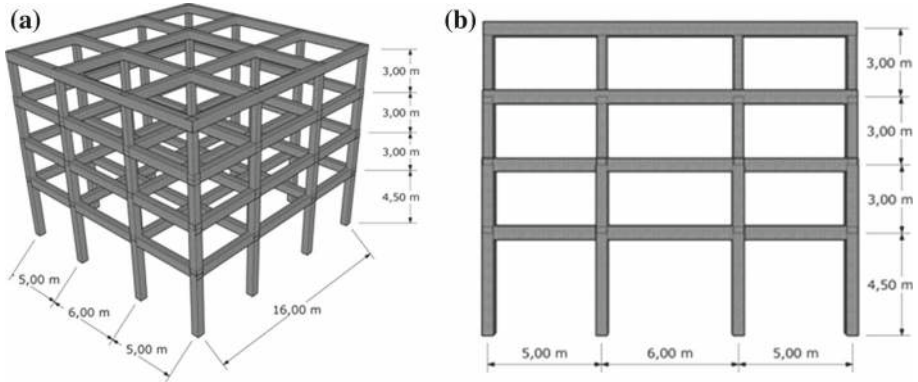


**Fig. 5** Geometry and model of the building: **a** 3D sketch; **b** 2D model

286 and using normalized displacements:

$$287 \quad K_N(\delta_N) = \frac{\overline{K_{NL}(\delta/\delta_u)}}{\overline{K_{NL}(\delta_u)}}; \quad 0 \leq \delta_N \leq 1; \quad 0 \leq K_N(\delta_N) \leq 1; \quad (17)$$

288  $K_N(\delta_N)$  is defined by the ratio between the stiffness variation with respect to the maximum,  
 289 and the total variation of stiffness. As the stiffness tends to decrease with increasing displac-  
 290 ement,  $K_N(\delta_N)$ , increases with the displacement so that is zero in the linear range and is one  
 291 at  $\delta_N = 1$ , that is at  $\delta = \delta_u$ .

292 Since, according to Eq. (12),  $DI_{PA}$  is a linear combination of a function that depends  
 293 on the displacement and a function that depends on the energy, the following new damage  
 294 index,  $DI_{CC}(\delta_N)$ , is defined:

$$295 \quad DI_{CC}(\delta_N) = aK_{NN}(\delta_N) + (1 - a)E_{NN}(\delta_N) \cong DI_{PA}(\delta_N) \quad (18)$$

296 where  $K_{NN}(\delta_N) = DI_{PA}(\delta_u) K_N(\delta_N)$ ,  $E_{NN}(\delta_N) = DI_{PA}(\delta_u) E_N(\delta_N)$  and for  $\delta_N = 1$

$$297 \quad K_{NN}(1) = E_{NN}(1) = DI_{PA}(\delta_u) \approx 1 \quad (19)$$

298 Thus,  $DI_{PA}$  can be used to calibrate the value of the parameter  $a$ . This new damage index  
 299 is called from now, capacity curve damage index,  $DI_{CC}(\delta_N)$ .  $K_N(\delta_N)$  and  $E_N(\delta_N)$  can  
 300 be calculated in a very simple way, both from the capacity curve and from the capacity  
 301 spectrum and, if the parametric model proposed above is available, these curves are also  
 302 fully determined by the lognormal or Beta functions of the capacity model. A practical  
 303 example of the computation and calibration of  $DI_{CC}$  is shown in the following.

### 304 3.2 Computation and calibration of the capacity curve damage index

305 The structure used for illustrating the practical computation of the damage model is a rein-  
 306 forced concrete building with four stories and frames with three spans. This building was  
 307 designed specifically for this work and it was also used in Vargas-Alzate (2013) to check  
 308 several techniques for calculating the seismic performance as well as various methods of damage  
 309 assessment. The main geometrical characteristics and the structural model are shown in  
 310 Fig. 5a. Due to its symmetry, the building is modeled as the two-dimension frame shown in  
 311 Fig. 5b. The characteristics of beams and columns are given in Table 3.

**Table 3** Characteristics of the structural model of Fig. 5

Storey	Columns			Beams		
	$b$ (m)	$h$ (m)	$\rho$	$b$ (m)	$h$ (m)	$\rho$
1	0.5	0.5	0.03	0.45	0.6	0.0066
2	0.5	0.5	0.02	0.45	0.6	0.0066
3	0.45	0.45	0.015	0.45	0.6	0.0066
4	0.4	0.4	0.015	0.45	0.6	0.0066

$b$ ,  $h$  and  $\rho$  are length, width and amount of steel of the cross-section of the structural element respectively

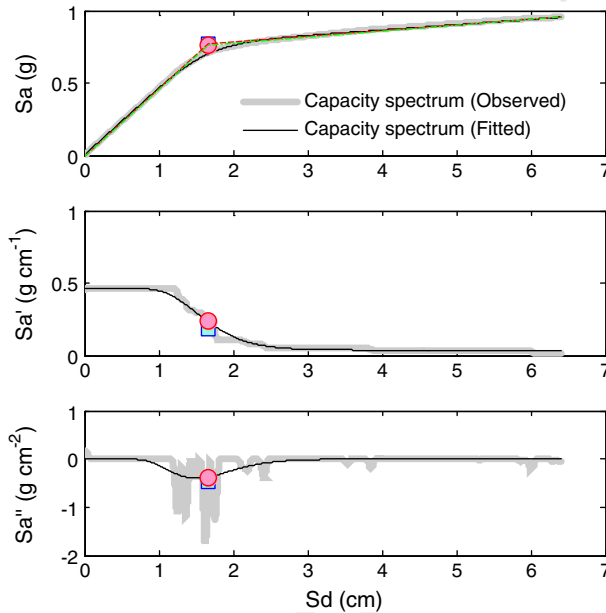


**Fig. 6** Capacity spectrum of the building of Fig. 5. The observed and modeled spectra are shown together with their first and second derivatives. Circle marker corresponds to the yielding point computed from the modeled spectrum, square marker corresponds to the one computed from the observed spectrum

312 The constitutive model used for beams and columns follows an elastoplastic hysteresis rule  
 313 with 5% hardening. Yielding surfaces are defined by the bending-compression interaction  
 314 diagram for columns and by the moment-curvature for beams.

315 The nonlinear behavior of the materials was considered by using the Takeda modified  
 316 hysteretic rule (Otani 1974). To construct the damping matrix, the Rayleigh method was  
 317 used. The loads were applied following the recommendations of Eurocode 2 for concrete  
 318 structures (BS EN 2005). The parametric model was applied to the pushover curve of the  
 319 building. Due to the normalizations involved in the fitting procedures, the model parameters  
 320 are the same for the capacity curve and for the capacity spectrum. Figure 6 shows the capacity  
 321 spectrum and the yielding point. The first and second derivatives of the capacity spectrum  
 322 are also shown in this figure.

323 The curves modeled by means of the lognormal function are also plotted. A good fit  
 324 also has been obtained with the Beta function. The errors are always lower than 2% for the  
 325 lognormal fit. Table 4 shows the parameters of the lognormal and Beta functions.

**Table 4** Parameters of the lognormal and Beta models for the capacity curve of Fig. 6

Lognormal				Beta			
$\mu$	$\sigma$	Mean ( $M_L$ )	Variance ( $V_L$ )	$\lambda$	$\nu$	Mean ( $M_B$ )	Variance ( $V_B$ )
0.254	0.27	0.263	0.0052	41.2	127.77	0.244	0.0011

The mean value and the variance of both distributions are also shown

**Table 5** Yielding ( $S_{dy}, S_{ay}$ ) and ultimate ( $S_{du}, S_{au}$ ) capacity points of the capacity spectrum of Fig. 6

$S_{dy_{fit}}$ (cm)	$S_{ay_{fit}}$ (g)	$S_{du}$ (cm)	$S_{au}$ (g)	$m$ (g/cm)	$T$ (s)
1.66	0.76	6.41	0.95	0.463	0.29

$fit$  stands for the fitted spectrum. The slope,  $m$ , of the linear part of the capacity curve and the fundamental period,  $T$ , of the building are also shown

The yielding point defining the bilinear capacity spectrum was calculated by using the actual and the fitted spectrum. Virtually the same point was obtained. Table 5 shows the yielding and the ultimate capacity points corresponding to the fitted spectrum, along with the slope and the period defining the linear part.

The Park and Ang index for this building was estimated by means of incremental dynamic analysis (Vamvatsikos and Cornell 2001). The Ruaumoko program (Carr 2000) was used to carry out the dynamic analyses. The seismic action was defined by means of an actual accelerogram whose response spectrum is compatible with the response spectrum provided by the Eurocode 8 (CEN 2004) for great earthquakes (type 1,  $M_S > 5.5$ ) and soft soil (soil class D). This spectrum is called herein as EC8 1D. The accelerogram was selected from the European strong motion database (Ambraseys et al. 2002, 2004) according to the procedure described in Vargas-Alzate et al. (2013b) and it corresponds to the Friuli earthquake (06/May/1976,  $M_w = 6.6$ , depth = 6 km) as recorded at an epicentral distance of 48 km. Figure 7 shows the accelerogram normalized at a Peak Ground Acceleration (PGA) of 1 g. In this figure, the Fourier amplitude spectrum and the 5% damped elastic response spectrum are also shown. For comparison purposes, the EC8 1D spectrum, together with the response spectrum of the accelerogram and the fundamental period of the building, is also shown in Fig. 7d.

Incremental dynamic analysis was performed scaling this accelerogram for PGA values between 0.01 and 0.9 g, with 0.01 g intervals. Figure 8a shows the  $DI_{PA}$ , the capacity curve and its bilinear form. Figure 8b shows the relationship obtained between PGA and the maximum displacement at the roof of the building,  $\delta$ . In these two figures, the thresholds of the damage states adopted in the Risk-UE project (Barbat et al. 2006a, b; Lagomarsino and Giovinazzi 2006) are also depicted. These damage states and thresholds are described below in the following section devoted to the fragility model.

Figure 9a shows how the new damage index,  $DI_{CCA}(\delta_N)$ , is calibrated by using the Park and Ang index,  $DI_{PA} IDA(\delta_N)$ , and the functions that define the energy index,  $E_{NNA}(\delta_N)$  and the stiffness index,  $K_{NNA}(\delta_N)$ . The subscript A in these functions indicates they were calculated directly from the actual capacity curve. Virtually identical results were obtained using the parametric model. The parameter,  $\alpha$ , was obtained by means of a least squares fit of Eq. (18). For the case discussed here,  $\alpha = 0.78$ . Figure 9b shows the differences between the new index  $DI_{CCA}(\delta_N)$  calculated from the actual capacity curve and  $DI_{PA} IDA(\delta_N)$ .

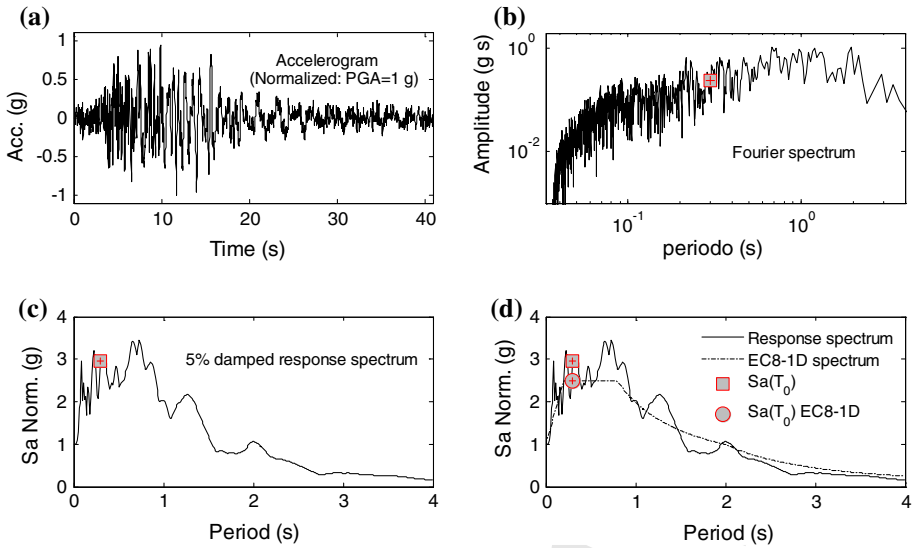


**Fig. 7** Accelerogram selected for the incremental dynamic analysis: **a** PGA normalized accelerogram; **b** Fourier amplitude spectrum; **c** 5% damped elastic acceleration response spectrum; **d** comparison between the accelerometer response spectrum and the EC8 1D spectrum. In **b–d** the fundamental period of the building is also shown

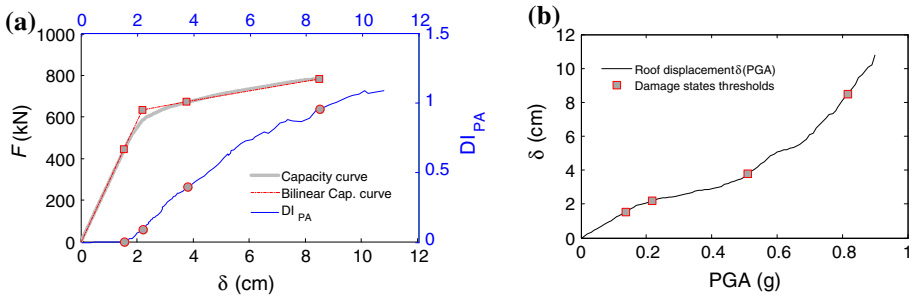


**Fig. 8** **a** Capacity curve and Park and Ang damage index,  $DI_{PA}$ . **b** Maximum displacement as a function of PGA. The damage states thresholds adopted from Risk UE project are also shown

358 The following three cases are shown in this figure: (1) differences between the new damage index,  $DI_{CCA}(\delta_N)$ , calculated from the actual capacity curve and the Park and Ang  
 359 index,  $DI_{PA\ IDA}(\delta_N)$ ; (2) differences between the new damage index,  $DI_{CCM}(\delta_N)$  calculated from the lognormal model and  $DI_{PA\ IDA}(\delta_N)$ ; and (3) differences between the new  
 360 index calculated from actual capacity curve,  $DI_{CCA}(\delta_N)$  and the one calculated from the lognormal model,  $DI_{CCM}(\delta_N)$ . Note the goodness of the fits when the actual capacity and  
 361 the lognormal model of the capacity curve are used. The maximum difference is lesser than 0.04 damage index units. The value of the parameter  $\alpha$  for the actual capacity curve is 0.78,  
 362 and 0.77 for the parametric model. The variances of the difference vectors are respectively 4.0E-5 and 6.5e-5 indicating the goodness of both fits. The differences between the new  
 363 damage indices calculated from the actual and from the modeled capacity curve are very  
 364 small too. The maximum difference is lesser than 0.02 damage index units. The parameter  $\alpha$   
 365  
 366  
 367  
 368  
 369

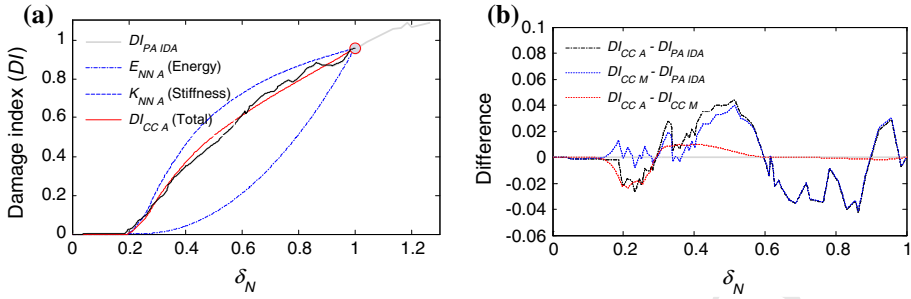


**Fig. 9** **a** Calibration of the new damage index  $DI_{CCA}$  obtained from the actual capacity curve. The Energy and stiffness functions are also displayed. Circle marker corresponds to the value of the Park and Ang index at  $\delta_N = 1$ . **b** Differences between the new damage indexes obtained from the actual,  $DI_{CCA}$ , and modeled,  $DI_{CCM}$ , capacity curves and the  $DI_{PAIDA}$ . The differences between the new damage index obtained from the actual and modeled capacity curve are also displayed

370 is crucial for the damage model. Observe that  $DI_{PAIDA}(\delta_N)$  is obtained for a specific seismic  
 371 action. It can be expected that different seismic actions will lead to different Park and Ang  
 372 indexes and, therefore, to different values of this important parameter. Thus the parameter  $\alpha$   
 373 allows the new index,  $DI_{CCM}(\delta_N)$ , properly fitting the response and the expected damage  
 374 when the building is subjected to different seismic actions. Ongoing work will contribute to  
 375 evaluate the sensitivity of this parameter to seismic actions with different response spectra  
 376 and with different durations.

#### 377 4 Fragility model

378 To assess the seismic expected damage, mechanical methods (Giovinazzi 2005; Lagomarsino  
 379 and Giovinazzi 2006) usually consider four non-null damage states: (1) *Slight*, (2) *Moderate*,  
 380 (3) *Severe* and (4) *Complete*. It is important to note that the *Complete* damage state has been  
 381 incorrectly identified at times as the state of *Collapse*. Actually, this damage state comes  
 382 from the union of the *Extensive* and *Collapse* damage states as defined, for instance, in the  
 383 European macroseismic scale (Grünthal 1998); to see how these damage states are used in  
 384 practical applications see also Lantada et al. (2010). So, the *Complete* damage state here  
 385 strictly means *Irreparable Damage*, that is, the condition of the building holding this damage  
 386 state, makes it more expensive to repair than to demolish and rebuild. For each damage state,  
 387 the corresponding fragility curve defines the probability of exceeding the damage state as a  
 388 function of the spectral displacement.

##### 389 4.1 The risk-UE model

390 In this section, the method for determining the damage states thresholds and the fragility  
 391 curves as proposed in the Risk-UE project (Milutinovic and Trendafiloski 2003) is analyzed  
 392 and discussed. This method has been used to assess the seismic damage and risk in European  
 393 cities (see for instance Lantada et al. 2009; Pujades et al. 2012). Lagomarsino and Giovinazzi  
 394 (2006) propose a simple technique that allows obtaining the four fragility curves from the  
 395 bilinear capacity spectrum through the following assumptions: (1) for each damage state,  
 396  $k$ , the corresponding fragility curve follows a lognormal cumulative distribution defined by  
 397 the parameters  $\mu_k$  and  $\beta_k$ ; consequently the value of the fragility curve at  $\mu_k$  is 0.5; (2) the

398 damage is distributed according to a binomial probability distribution and (3)  $\mu_k$  thresholds  
 399 are defined from the bilinear capacity spectrum according to the following equations:

400 
$$\mu_1 = 0.7 Dy \quad \mu_2 = Dy; \quad \mu_3 = Dy + 0.25(Du - Dy); \quad \mu_4 = Du \quad (20)$$

401 and, using the normalized form by dividing this equation by  $Du$ , leads to:

402 
$$\mu_{N1} = 0.7 Dy_N; \quad \mu_{N2} = Dy_N; \quad \mu_{N3} = Dy_N + 0.25(1 - Dy_N) = 0.25 + 0.75Dy_N;$$
  
 403 
$$\mu_{N4} = 1 \quad (21)$$

404 Assumption 2 is based on damage observed in real earthquakes (Grünthal 1998) and it allows  
 405 determining the damage states probabilities at each damage state threshold; assumption 3 is  
 406 based on expert opinion. Besides, assumptions (2) and (3) allow obtaining the values of the  
 407 four fragility curves at each damage state threshold,  $\mu_k$  or  $\mu_{Nk}$ . The details of the construction of fragility curves  
 408 allows obtaining the corresponding  $\beta_{Nk}$ . The details of the construction of fragility curves  
 409 are well explained in Lantada et al. (2009) and in Pujades et al. (2012). Figure 10 shows  
 410 the fragility curves corresponding to the capacity spectrum of Fig. 8a, but using normalized  
 411 values. The points used for the least squares fits are also shown in this figure. The parameters  
 412 of the fragility curves are shown in Table 6. Once the fragility curves,  $F_k(Sd)$ ,  $k = 1, \dots, 4$ ,  
 413 are known, for each spectral displacement,  $Sd$ , damage states histograms,  $P_j(Sd)$ , define the  
 414 probability of the damage state  $j$ . Equation (22) shows how these probabilities are obtained  
 415 from fragility curves:

416 
$$P_0(Sd) = 1 - F_1(Sd); \quad P_j(Sd) = F_j(Sd) - F_{j+1}(Sd) \quad j = 1, \dots, 3; \quad P_4(Sd) = F_4(Sd); \quad (22)$$

417 The following equation defines the mean damage state  $\overline{D(Sd)}$  and the normalized mean  
 418 damage state,  $MDS(Sd)$ :

419 
$$\overline{D(Sd)} = \sum_{i=0}^4 i P_i(Sd) = 4 MDS(Sd) \quad (23)$$

420  $\overline{D(Sd)}$  takes values between 0 (no damage) and 4 (Complete damage state);  $MDS(Sd)$  is  
 421 obtained by dividing the mean damage state by the number of non-null damage states, namely  
 422 by 4 in this case.  $MDS(Sd)$  takes values between zero (no damage) and 1 (Complete damage  
 423 state). In turn, this normalized mean damage state is the parameter of the binomial distrib-  
 424 ution that defines the probabilities  $P_i(Sd)$ ,  $i = 0, \dots, 4$ , so that unambiguously determines  
 425 the damage states histograms and, by using Eq. (22), the fragility curves. For easier compar-  
 426 427 ison with the following developments, normalized spectra, normalized fragility curves  
 428 and normalized mean damage states will be used from now. Figure 10 shows the obtained  
 429 fragility curves,  $F_j(Sd_N)$ , and the normalized mean damage state,  $MDS$  as a function of the  
 430 normalized spectral displacement  $Sd_N$

431 The correlation between the Park and Ang damage index,  $DI_{PA}$ , and the Risk UE based  
 432 mean damage state,  $MDS$  in Fig. 10, must be tackled carefully because their senses are  
 433 different. Obviously both are related to damage but  $MDS$  has a statistical meaning while  
 434  $DI_{PA}$  must be interpreted as a physical pointer. Risk-UE based thresholds are defined by  
 435 those displacements for which the probability of exceeding the corresponding damage state  
 436 is 50% and its simplified definition from capacity curve is based on expert opinion. In turn,  
 437 no doubt, the expert opinion is based on the progressive degradation of the bearing capacity  
 of the building. This delicate discussion will be resumed below.

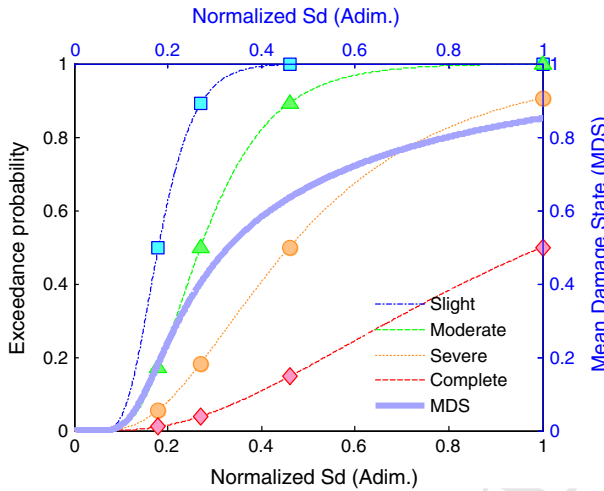


**Fig. 10** Fragility curves and mean damage state for the building of Fig. 5

#### 4.2 Fragility curves based on the new damage index

Park et al. (1985) calibrated the  $DI_{PA}$  index from damage observed in nine reinforced concrete buildings, concluding that  $DI_{PA} \leq 0.4$  corresponds to a repairable damage,  $DI_{PA} > 0.4$  denotes a damage level making the building difficult to repair and  $DI_{PA} \geq 1.0$  represents total collapse. In later works (Park et al. 1985; Cosenza and Manfredi 2000) it was found out that  $DI_{PA} \geq 1.0$  implies the collapse, for  $DI_{PA} \leq 0.5$  the damage is repairable and for  $0.5 < DI_{PA} < 1$  the collapse of the building does not occur but the building cannot be considered repairable. Moreover, when  $DI_{PA} < 0.2$  it is considered that the damage is negligible. So, based on these results, critical values of the Park and Ang damage index have been used to propose new damage states thresholds. Specifically, the normalized displacements corresponding to damage indices of 0.05, 0.2, 0.4, and 0.65 have been allotted respectively to the thresholds of the damage states *Slight*, *Moderate*, *Severe*, and *Complete*. It is worth to recall that the *Complete* damage state means here not-repairable-damage. The probabilities of exceedance at the damage states thresholds are kept at 0.5. To find these thresholds we have used the  $DI_{PA IDA}$  and the new  $DI_{CC}$  index obtained from the capacity curve. Results obtained using the actual capacity curve and the modeled according to the model proposed here are almost identical. So only the results obtained from the actual capacity curve,  $DI_{CC A}$ , are shown here. Table 6 shows the parameters of the fragility curves corresponding to the following three cases: (1) Risk-UE based fragility curves, (2) fragility curves based on the  $DI_{PA IDA}$  and 3) fragility curves based on the new  $DI_{CC A}$  damage index. The  $\mu_{Nk}$  and  $\beta_{Nk}$  of the four normalized fragility curves are given in this table. The variances of the fits are also shown.

Figure 11a shows the fragility curves corresponding to the case based on the new  $DI_{CC A}$  damage states thresholds. The corresponding mean damage state function (MDS) is also shown in this figure. The Risk-UE based case has been shown above in Fig. 10. Figure 11b compares the mean damage states functions, as defined in Eqs. (22) and (23), corresponding to the three cases. The mean damage state function corresponding to the fragility curves whose damage states thresholds have been fixed using the  $DI_{PA IDA}$  and from the  $DI_{CC A}$  are virtually identical. The values of the mean damage state functions (MDS) at the damage states



**Table 6** Parameters which define the fragility curves based on the Risk-UE,  $DI_{PA\ IDA}$  and  $DI_{CC\ A}$  damage states thresholds

Type	1: <i>Slight</i>			2: <i>Moderate</i>			3: <i>Severe</i>			4: <i>Complete</i>		
	$\mu_{N1}$	$\beta_{N1}$	$V_{N1}$	$\mu_{N2}$	$\beta_{N2}$	$V_{N2}$	$\mu_{N3}$	$\beta_{N3}$	$V_{N3}$	$\mu_{N4}$	$\beta_{N4}$	$V_{N4}$
Risk-UE	0.18	0.34	0.1E-3	0.27	0.42	2.1E-3	0.43	0.59	1.1E-3	1.0	1.0	0.10E-3
$DI_{PA\ IDA}$	0.23	0.32	0.2E-3	0.32	0.32	0.2E-3	0.44	0.31	0.1E-3	0.63	0.33	0.03E-3
$DI_{CC\ A}$	0.22	0.33	0.2E-3	0.32	0.30	0.3E-3	0.43	0.33	0.1E-3	0.64	0.37	0.02E-3

The variances  $V_{Nk}$  of the fits are also given

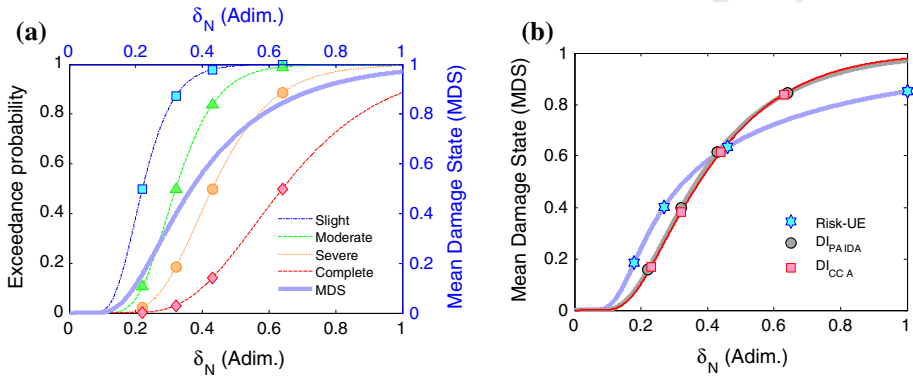


**Fig. 11** **a** Fragility curves and MDS function obtained by using the damage states thresholds based on the new  $DI_{CC\ A}$ . **b** Comparison of the mean damage state functions

467 thresholds are also shown in Fig. 11b. It can be seen how the Risk-UE based mean damage  
 468 state function overestimates the damage beneath the *Severe* damage state and underestimates  
 469 the expected damage above this damage state threshold. It is worth noting that beneath *Severe*  
 470 damage state, Risk-UE damage model overestimates the expected damage because it takes  
 471 into account that some damage occurs also in the linear branch of the capacity curve due  
 472 to non-structural elements. Above this damage state, in later versions of the Risk-UE based  
 473 damage models (see for instance [Giovinazzi 2005](#); [Lagomarsino and Giovinazzi 2006](#)), the  
 474 damage states thresholds have been shifted to consider non-reparable damage. Otherwise,  
 475 this disagreement can also be reduced by assigning other Park and Ang index values to the  
 476 damage states thresholds. In the case here analyzed, the values of the Park and Ang indices  
 477 corresponding to the Risk-UE damage states thresholds are 0.002, 0.1, 0.4 and 0.9, instead of  
 478 0.05, 0.2, 0.4 and 0.65, respectively for the *Slight*, *Moderate*, *Severe* and *Complete* damage  
 479 states. As we will discuss later on, in our view, these expert opinion based decisions need  
 480 further analyses and calibration.

481 **5 Usefulness of the model**

482 Due to improvements in computational capabilities the use of nonlinear time history analysis,  
 483 is increasing so that it could be argued that the capacity spectrum method is less popular  
 484 these days than it has been and, therefore, the usefulness of the models here proposed for  
 485 the current earthquake engineering research or practice could be questioned. In this respect,

486 Gencturk and Elnashai (2008) claim that notwithstanding that it is the most accurate method  
 487 of earthquake assessment, inelastic dynamic analysis is not always feasible owing to the  
 488 involved computational and modeling effort, convergence problems and complexity. This is  
 489 one of the reasons why nonlinear static analysis is still preferred and new improvements are  
 490 proposed (Fajfar et al. 2005a, b; Casarotti and Pinho 2007; Pinho et al. 2008, 2009). Moreover,  
 491 nonlinear static procedures can be applied even to asymmetric 3D buildings (Chopra and Goel  
 492 2004; Bhatt and Bento 2011, 2013). Therefore, the availability of a new mathematical model  
 493 for capacity curves/spectra can be a powerful tool for current earthquake engineering research  
 494 or practice. This is particularly true in probabilistic assessments of structures (Vargas-Alzate  
 495 et al. 2013a, b, c, d) involving hundreds or even thousands of nonlinear structural analyses.  
 496 In fact it is in the framework of such kind of analyses that the models here presented were  
 497 conceived. Indeed the model permits to simulate, in a straightforward manner, any type  
 498 of capacity spectrum allowing classifying great amounts of buildings to set up complete  
 499 parametric definitions of building typology matrices as well as to tabulate critical points of  
 500 capacity spectra to be used in massive computations. In fact, the model has been tested on a  
 501 large collection of capacity curves, both actual and synthetic, with excellent results in all the  
 502 cases, showing a great usefulness, versatility and robustness.

503 In the following several examples of the usefulness of the models are shown. The first  
 504 one allows obtaining empirical functions linking the parameters of the capacity model to the  
 505 maximum structural ductility; in this framework a new easy method to estimate the yielding  
 506 point and indeed the maximum ductility is proposed. The second one allows examining how  
 507 elastoplastic, hardening and softening capacity curves/spectra may share the same nonlinear  
 508 part and indeed the same degradation, damage and fragility models. However, it also must  
 509 be noted that, for a given seismic action defined by its 5% damped response spectrum, the  
 510 damage expected will be different because the spectral displacement of the performance  
 511 point also depends on the other two parameters that define the full capacity model, namely  
 512 the initial slope,  $m$ , or the fundamental period  $T$ , and the spectral acceleration,  $A_u$ , at the  
 513 ultimate capacity point and, therefore, the damage expected depends on the overall shape  
 514 of the capacity spectrum. Finally two less usual cases concerning to buildings with singular  
 515 capacity spectra are presented to show the ability of the model to deal also with these kinds  
 516 of capacity spectra.

## 517 5.1 Yielding point and ductility

518 As stated in the Introduction, the bilinear form of a capacity spectrum is defined by the yield-  
 519 ing point,  $(D_y, A_y)$ , and the ultimate capacity point,  $(D_u, A_u)$ . Remind that an important  
 520 condition to be fulfilled is that the areas under the capacity spectrum and its bilinear form  
 521 must be the same. In this subsection we show how  $D_y$  also can be obtained from the nor-  
 522 malized nonlinear part of the capacity spectrum. Indeed, both the capacity spectrum and its  
 523 bilinear form can be decomposed into their linear and nonlinear parts. Meanwhile, the linear  
 524 part is the same for both curves and the nonlinear part of the bilinear form is a simple triangle,  
 525 whose area should be equal to the area under the curve that defines the nonlinear part of the  
 526 capacity spectrum. Let  $S_C$  and  $S_B$  be respectively the areas under the capacity spectrum and  
 527 under its nonlinear part; in turn, let  $S_{C_L}$ ,  $S_{B_L}$ ,  $S_{C_{NL}}$  and  $S_{B_{NL}}$  be the respective areas  
 528 of the linear and nonlinear parts. Given that the capacity spectrum,  $C$ , and its linear,  $C_L$ , and  
 529 nonlinear,  $C_{NL}$ , parts meet the condition  $C_{NL} = C - C_L$ , the following equation is fulfilled:

$$\begin{aligned}
 530 \quad S_{C_{NL}} &= S_{C_L} - S_C \quad \text{for the capacity spectrum} \\
 531 \quad S_{B_{NL}} &= S_{B_L} - S_B \quad \text{for the bilinear form}
 \end{aligned} \tag{24}$$

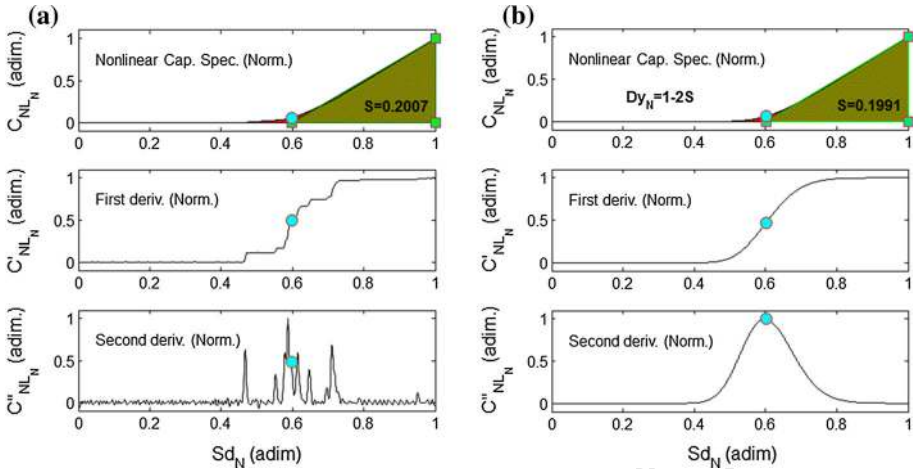


**Fig. 12** Illustration of the new method to obtain  $Dy_N$ : **a** For the capacity spectrum of Fig. 1; **b** For the model fitted. The *circle* corresponds to the yielding point; *squares* define the triangle used to compute the area  $S_{BN\_NL}$  in Eq. (26)

532 Taking into account that  $S_C$  and  $S_B$  must be equal and that the linear parts  $S_{C\_L}$  and  $S_{B\_L}$  are  
 533 identical, the condition over the areas of Eq. (24) is reduced to  $S_{C\_NL} = S_{B\_NL}$ . Equations  
 534 (24) also apply to curves normalized in both axes, given that normalized curves are obtained  
 535 by dividing by the same constant of normalization in both sides of these equations. Moreover,  
 536 calling  $Dy_N$  the normalized spectral displacement of the yielding point,  $S_{BN\_NL}$  the area  
 537 under the normalized nonlinear part of the bilinear spectrum and  $S_{CN\_NL}$  the area under the  
 538 normalized nonlinear part of the capacity spectrum, it is verified that:

$$539 \quad S_{BN\_NL} = (1 - Dy_N)/2 \Rightarrow Dy_N = 1 - 2S_{BN\_NL} = 1 - 2S_{CN\_NL} \quad (25)$$

540 Thus, the yielding point of the bilinear capacity spectrum can be calculated easily using the  
 541 following steps: (1) use Eq. (1), or Eq. (6) for the modeled curve, to calculate the normalized  
 542 nonlinear part of the capacity spectrum; note that this step also implies normalizing abscissae  
 543 and ordinates; (2) calculate the area under this curve and use Eq. (25) to get  $Dy_N$ ; (3) finally,  
 544  $Dy$ ,  $Ay$  and  $q$  are obtained by using the following equations:

$$545 \quad Dy = Dy_N Du; \quad Ay = m Dy; \quad q = Du/Dy = 1/Dy_N \quad (26)$$

546 where  $q$  is the ductility factor. For the empirical capacity spectrum of Fig. 1 the same value  
 547  $Dy_N = 0.599$  is obtained when computed by means of the conventional technique and by  
 548 means of the new method here proposed. If we use the model that fits this curve (parameters  
 549 in Table 2), this value is 0.602. The values obtained by means of the classical and the  
 550 new method match perfectly. Moreover, the differences between the values obtained for the  
 551 actual and modeled spectrum are 0.5%, showing the goodness of both the model and the  
 552 new calculation method. Figure 12 illustrates the new simpler method to calculate  $Dy_N$ .  
 553 Figure 12a corresponds to the actual spectrum shown in Fig. 1, whereas Fig. 12b shows the  
 554 case of the modeled spectrum using the lognormal model with parameters  $\mu = 0.608$  and  
 555  $\sigma = 0.12$  (Table 2). In Fig. 12, the normalized nonlinear capacity spectrum and its bilinear  
 556 form are shown.

557 It can be seen the two areas to be equaled. Figures at the middle and bottom show the first  
 558 and second derivatives, normalized, of the nonlinear part of the capacity spectrum. Circle

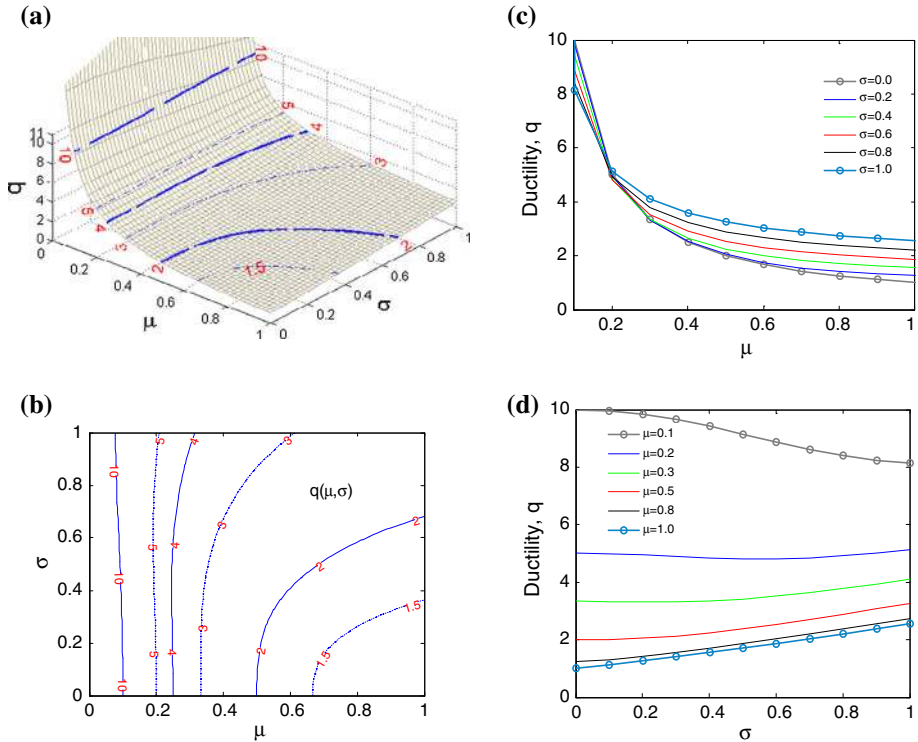


**Fig. 13** Ductility  $q$  as a function of the parameters  $\mu$  and  $\sigma$  that define the model for capacity curves: **a** surface showing the three parameters; **b** iso- $q$  curves; **c** iso- $\sigma$  curves; **d** iso- $\mu$  curves

559 marker in these figures show the position of the normalized yielding point  $D_{yN}$ . Note that  
 560  $D_{yN}$  is very close to the  $\mu$  value, but not identical. In fact low  $\sigma$  values lead to  $D_{yN}$  similar to  
 561  $\mu$ . As  $\mu$  and  $\sigma$  increase the differences between  $D_{yN}$  and  $\mu$  also increase. So, for instance, for  
 562  $\mu = 0.608$  and  $\sigma = 0.8$ ,  $D_{yN}$  is equal to 0.354 and for  $\mu = 0.85$  and  $\sigma = 0.8$ ,  $D_{yN}$  is equal  
 563 to 0.4. Moreover, the simplicity of the model allows to establish an easy relationship between  
 564 the lognormal distribution parameters,  $\mu$  and  $\sigma$ , and the normalized yielding displacement,  
 565  $D_{yN}$ , or equivalently, between  $\mu$ ,  $\sigma$  and the ductility,  $q$ . Since the determination of  $D_{yN}$   
 566 requires a double integration of the lognormal probability density function, these relationships  
 567 will be non-parametric. These non-parametric functions are plotted in Fig. 13 and tabulated  
 568 in Table 7 for the maximum ductility factor  $q$ .

569 It is worth noting that, since we have shown that the ductility factor  $q$ , or  $D_{yN}$ , depends  
 570 only on  $\mu$  and  $\sigma$ , all the capacity spectra with the same model and the same  $Sd_u$ , have the  
 571 same  $Sd_y$ , regardless of the parameters  $Sa_u$  and  $m$ , and vice versa. This remark is important,  
 572 given that it shows that all the capacity curves with the same model have the same degradation  
 573 pattern, and indeed the same fragility curves.

574 To deepen this statement, different kinds of capacity spectra holding the same parametric  
 575 model are shown in the following subsection. However, as argued above, we have to remind  
 576 that, for a given seismic action, the performance point and therefore the damage expected,  
 577 depends on the shape of the whole capacity spectrum.

**Table 7** Values of the ductility factor,  $q$ , as a function of the parameters  $\mu$  and  $\sigma$  that define the model for capacity curves

$\mu$ values	$\sigma$ values																			
	0.050	0.100	0.150	0.200	0.250	0.300	0.350	0.400	0.450	0.500	0.550	0.600	0.650	0.700	0.750	0.800	0.850	0.900	0.950	1.000
0.050	16.13	16.13	16.13	16.13	16.10	16.00	15.84	15.61	15.34	15.03	14.70	14.35	14.00	13.64	13.29	12.94	12.61	12.30	12.00	11.72
0.100	10.14	10.14	10.13	10.04	9.90	9.74	9.56	9.38	9.20	9.02	8.85	8.67	8.51	8.35	8.21	8.08	7.96	7.87	7.78	7.71
0.150	6.73	6.73	6.69	6.63	6.58	6.53	6.47	6.41	6.34	6.27	6.20	6.14	6.09	6.05	6.01	5.99	5.98	5.98	5.99	6.00
0.200	5.04	5.03	5.00	4.98	4.95	4.93	4.90	4.87	4.85	4.83	4.82	4.82	4.83	4.84	4.87	4.90	4.93	4.98	5.03	5.08
0.250	4.03	4.01	4.00	3.99	3.98	3.97	3.97	3.96	3.97	3.98	4.00	4.04	4.07	4.12	4.17	4.23	4.29	4.36	4.43	4.50
0.300	3.35	3.34	3.34	3.34	3.34	3.34	3.35	3.37	3.39	3.43	3.47	3.52	3.58	3.64	3.71	3.78	3.86	3.94	4.02	4.10
0.350	2.87	2.87	2.87	2.88	2.88	2.90	2.92	2.95	2.99	3.04	3.10	3.16	3.23	3.31	3.39	3.47	3.55	3.63	3.72	3.81
0.400	2.51	2.51	2.52	2.53	2.55	2.57	2.61	2.65	2.70	2.76	2.83	2.90	2.98	3.06	3.14	3.23	3.31	3.40	3.49	3.58
0.450	2.23	2.24	2.25	2.26	2.29	2.32	2.37	2.42	2.48	2.55	2.62	2.70	2.78	2.87	2.95	3.04	3.13	3.22	3.31	3.41
0.500	2.01	2.02	2.03	2.05	2.09	2.13	2.18	2.25	2.31	2.39	2.46	2.54	2.63	2.71	2.80	2.89	2.98	3.07	3.17	3.26
0.550	1.83	1.84	1.86	1.89	1.93	1.98	2.04	2.11	2.18	2.26	2.34	2.42	2.50	2.59	2.68	2.77	2.86	2.95	3.05	3.14
0.600	1.68	1.69	1.71	1.75	1.80	1.86	1.92	2.00	2.07	2.15	2.23	2.31	2.40	2.49	2.58	2.67	2.76	2.85	2.94	3.04
0.650	1.55	1.57	1.60	1.64	1.70	1.76	1.83	1.90	1.98	2.06	2.14	2.23	2.31	2.40	2.49	2.58	2.67	2.76	2.86	2.95
0.700	1.44	1.46	1.50	1.55	1.61	1.68	1.75	1.83	1.91	1.99	2.07	2.15	2.24	2.33	2.42	2.50	2.60	2.69	2.78	2.87
0.750	1.35	1.37	1.42	1.48	1.54	1.62	1.69	1.77	1.84	1.92	2.01	2.09	2.18	2.26	2.35	2.44	2.53	2.62	2.71	2.80
0.800	1.27	1.30	1.36	1.42	1.49	1.56	1.63	1.71	1.79	1.87	1.95	2.04	2.12	2.21	2.29	2.38	2.47	2.56	2.65	2.74
0.850	1.20	1.25	1.31	1.37	1.44	1.51	1.59	1.67	1.74	1.82	1.91	1.99	2.07	2.16	2.24	2.33	2.42	2.51	2.60	2.69
0.900	1.15	1.20	1.26	1.33	1.40	1.48	1.55	1.63	1.70	1.78	1.86	1.95	2.03	2.11	2.20	2.29	2.37	2.46	2.55	2.64
0.950	1.11	1.17	1.23	1.30	1.37	1.44	1.52	1.59	1.67	1.75	1.83	1.91	1.99	2.07	2.16	2.25	2.33	2.42	2.51	2.60
1.000	1.08	1.14	1.20	1.27	1.34	1.41	1.49	1.56	1.64	1.71	1.79	1.87	1.96	2.04	2.12	2.21	2.29	2.38	2.47	2.56

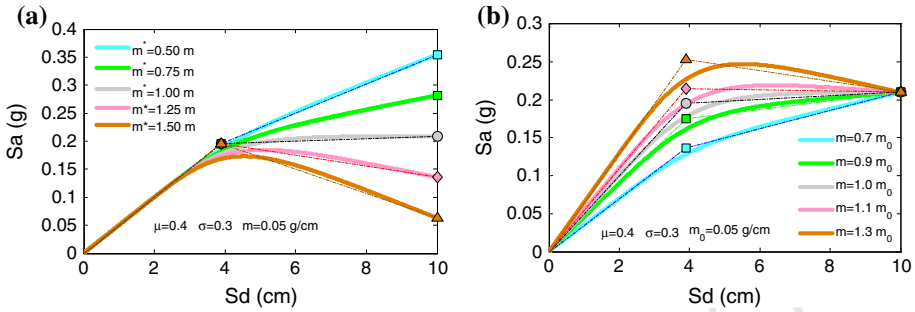


**Fig. 14** Examples of synthesis of capacity spectra with identical  $\mu$  and  $\sigma$ : **a**  $m$  constant and  $m^*$  variable; **b**  $m$  variable and  $S_{a_u}$  constant

578 5.2 Elastoplastic, hardening and softening models

579 The slope,  $m^*$ , at the end of the nonlinear capacity spectrum is another interesting parameter.  
 580 It can be shown that  $m^*$  and the slope,  $m_{CF}$ , at the end of the capacity spectrum are related as:  
 581  $m_{CF} = m - m^*$ . Thus  $m_{CF}$  is positive, null and negative for  $m > m^*$ ,  $m = m^*$  and  $m < m^*$ ,  
 582 respectively. In structural analysis, these three cases are typified as stiffness degradation  
 583 models, namely and respectively, softening (SO), elastoplastic (EP) and hardening (HA)  
 584 models. Furthermore,  $m^*$  is not an independent parameter, since it satisfies the following  
 585 equation:

$$m^* = \frac{C}{D}(m S_{d_u} - S_{a_u}) \tag{27}$$

587 C is the value of the cumulative lognormal function with parameters  $\mu$  and  $\sigma$  at  $x = 1$ , and D  
 588 is the value of the integral of the cumulative lognormal function also at  $x = 1$  but now scaled  
 589 at  $S_{d_u}$ . Thus, C and D are calculated directly, from  $\mu$ ,  $\sigma$  and  $S_{d_u}$ . The other parameters of  
 590 the Eq. (27) are known. Alternatively,  $m^*$  may be considered as independent parameter and  
 591  $S_{a_u}$  as dependent. Figure 14a shows the case for  $m$  constant and  $m^*$  variable. Figure 14b  
 592 shows the case for  $m$  variable and  $S_{a_u}$  constant. In both cases the bilinear spectra are also  
 593 shown. The patterns for SO, EP and HA models can be clearly seen in this figure. Table 8  
 594 shows the numerical values of the parameters involved.

595 Note how the same function, defined by parameters  $\mu$  and  $\sigma$ , may represent large families  
 596 of capacity spectra, also with identical  $S_{d_y}$  and  $S_{d_u}$  values, and vice versa.

597 5.3 Special cases

598 The usefulness of the model for more complex capacity spectra is shown herein. The first  
 599 case corresponds to a spectrum showing neither clear linear portion nor yielding point and  
 600 exhibiting negative tangent stiffness (softening) after the post-peak response. These types of  
 601 capacity spectra correspond to relatively low  $\mu$  and, in particular, to high  $\sigma$  values. Figure 15  
 602 shows the case of  $\mu = 0.3$  and  $\sigma = 1$ ; the other three parameters defining this capacity  
 603 spectrum are  $S_{d_u} = 10$  cm,  $S_{a_u} = 0.56$  g and the initial tangent stiffness corresponds  
 604 to a slope  $m = 0.25$  g/cm. Concerning to the bilinear capacity spectrum, in these cases it  
 605 is frequent to use a slope corresponding to an initial secant stiffness. Figure 15 shows the  
 606 capacity spectrum together with its linear and nonlinear parts. Two bilinear spectra are also  
 607 shown in this figure. The slope of the first branch of the first bilinear capacity spectrum  
 608 corresponds to the tangent stiffness, while that of the second one is  $m = 0.20$  g/cm that

Author Proof

**Table 8** Parameters of the capacity spectra of Fig. 14

	Independent parameters				Dependent parameters			Type	
	$\mu$	$\sigma$	$m$ (g/cm)	$Sdu$ (cm)	$Sau$ (g)	$Sdy$ (cm)	$Say$ (g)		$m^*$ (g/cm)
Figure 14a	0.4	0.3	0.050	10	0.354	3.89	0.195	0.025	HA
					0.282			0.038	HA
					0.209			0.050	EP
					0.136			0.062	SO
					0.063			0.075	SO
Figure 14b	0.4	0.3	0.035	10	0.210	3.89	0.137	0.024	HA
			0.045		0.176		0.041	HA	
			0.050		0.195		0.050	EP	
			0.055		0.215		0.058	SO	
			0.065		0.254		0.076	SO	

HA hardening, SO softening, EP elastoplastic

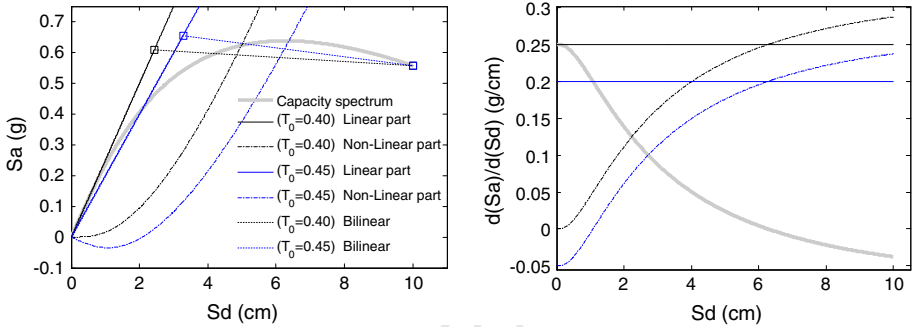


**Fig. 15** Parametric model for a capacity spectrum that gradually softens, showing neither clear linear portion nor yielding point, and exhibiting negative stiffness (softening) after the post-peak response (left) and corresponding first derivatives (right)

609 corresponds to a secant stiffness. As discussed above, these slopes can be also defined by the  
 610 corresponding periods being 0.40 and 0.45 respectively for the tangent and secant cases. Note  
 611 that even when initial secant stiffness is preferred for the bilinear capacity spectrum, Eqs. (25)  
 612 and (26) can be used to obtain the yielding point, but considering a kind of pseudo-non-linear  
 613 part obtained by considering the linear component with the secant stiffness chosen. As it can  
 614 be seen in Fig. 15, this procedure leads to obtain negative nonlinear parts leading to negative  
 615 areas which must be subtracted from positive contributions, so that different secant stiffness's  
 616 lead to different  $S_{CN\_NL}$  areas and indeed to different normalized yielding displacements  
 617  $Dy_N$ .

618 As it can be seen in Fig. 15, the yielding points ( $Dy$ ,  $Ay$ ) are (2.40 cm, 0.61 g) and  
 619 (3.27 cm, 0.66 g) respectively for the tangent and secant cases. All these curves can be  
 620 seen in Fig. 15 as well as the first derivatives of the capacity spectrum and of the linear and  
 621 nonlinear parts for the tangent and secant bilinear cases. However to fit the capacity curve,  
 622 whichever model is preferred, lognormal or Beta, the use of the tangent initial stiffness  
 623 corresponding to the fundamental period of the building is mandatory.

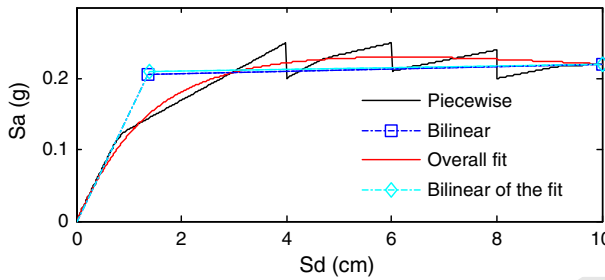


**Fig. 16** Synthetic piecewise capacity spectrum. The parameters of the piece functions are shown in Table 9

**Table 9** Parameters of the piecewise capacity spectrum of Fig. 16

Piece No.	Parameters defining the four piecewise functions							
	$S_{di}$ (cm)	$S_{du}$ (cm)	$S_{ai}$ (g)	$S_{au}$ (g)	$m$	$m^*$	$\mu$ (cm)	$\sigma$
1	0.0	4.0	0.00	0.25	0.150	0.040	0.20	0.12
2	4.0	6.0	0.20	0.25	0.040	0.017	0.34	0.2
3	6.0	8.0	0.21	0.24	0.017	0.016	0.20	0.2
4	8.0	10.0	0.20	0.22	0.016	0.003	0.60	0.05
Overall fit	0.0	10.0	0.00	0.22	0.150	-0.004	0.12	0.92

The parameters of each of the four piece-functions are shown. The parameters of the fit of the overall capacity spectrum are also included. See the explanation of the parameters in the text

624 The second special case corresponds to capacity spectra showing abrupt losses of strength  
 625 that usually are caused by partial failures of structural elements of the buildings. These  
 626 capacity spectra, common in the literature, can be defined by piecewise functions and, each  
 627 part or piece may be fitted by using the parametric model here proposed. Then, as many  
 628 as desired pieces can be joined properly to get the overall capacity spectrum. Obviously  
 629 a mean model for the whole capacity spectrum can be also obtained. Figure 16 shows a  
 630 synthetic typical case of this kind of capacity spectrum. Table 9 shows the parameters that  
 631 define each piece-function. In this table  $S_{di}$ ,  $S_{ai}$ ,  $S_{du}$  and  $S_{au}$  are the initial and final spectral  
 632 displacements and accelerations of each piece function;  $m$  and  $m^*$  are respectively the initial  
 633 and final slopes of each piece of capacity spectrum, as defined above;  $\mu$  and  $\sigma$  are the  
 634 parameters of the lognormal model defining the corresponding nonlinear part of each piece-  
 635 function. The parameters of the fit of the overall capacity spectrum also are included in this  
 636 table and the corresponding plot can be seen in Fig. 16. However, it is not self-evident that  
 637 it is possible to use, and how, stepwise functions.

## 638 6 Probabilistic capacity and damage models

639 The building of Fig. 5 is now used to deal with the problem from a probabilistic point of  
 640 view (Vargas-Alzate et al. 2013b, c, d; Barbat et al. 2013). This way, the application of the  
 641 capacity and damage models to more than one case can be shown and the uncertainties  
 642 involved can be estimated as well. The concrete compressive strength,  $f_c$ , and the steel yield  
 643 strength,  $f_y$ , have been modeled as normal random variables with respectively mean values  
 644 and standard deviations of 30 and 1.5 Mpa for  $f_c$  and 420 and 21 Mpa for  $f_y$ . The same



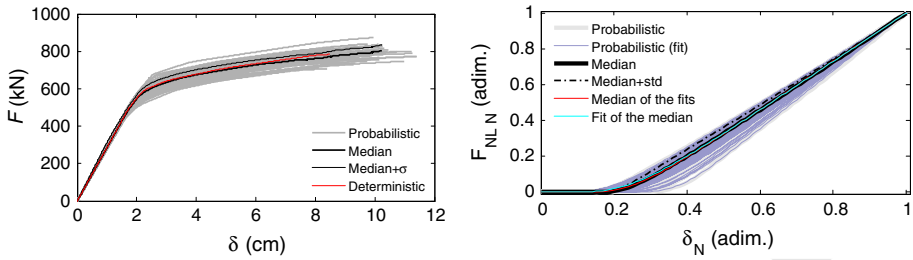


**Fig. 17** Probabilistic capacity curves (*left*) and corresponding normalized nonlinear parts

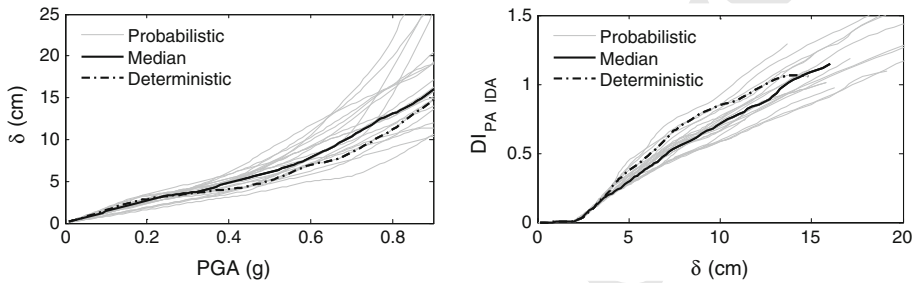


**Fig. 18** Maximum displacement as functions of the PGA (*left*) and corresponding Park and Ang damage indices,  $DI_{PA IDA}$  (*right*)

645 probability distributions were used by Vargas-Alzate et al. (2013b). Then, one hundred of  
 646 probabilistic capacity curves have been generated by means of Monte Carlo simulations. We  
 647 refer to the capacity curve of Fig. 8 as deterministic curve. Figure 17 shows the capacity  
 648 curves obtained. The median capacity curve, the median plus one standard deviation (SD)  
 649 and the deterministic curves are also depicted. Figure 17 also shows the normalized nonlinear  
 650 capacity curves ( $F_{NLN}$ ).

651 Concerning to the damage model, the building corresponding to the deterministic capacity  
 652 curve has been submitted to incremental dynamic analyses by using the 20 seismic actions  
 653 described in Vargas-Alzate et al. (2013b). These seismic actions were selected from the  
 654 European strong motion database (Ambraseys et al. 2002, 2008) in such a way that they  
 655 were compatible with the EC8 1D spectrum shown in Fig. 7. The characteristics of these  
 656 20 accelerograms are described in the appendix of Vargas-Alzate et al. (2013b). The roof  
 657 displacement,  $\delta$ , and the Park and Ang damage index,  $DI_{PA IDA}$ , have been obtained for each  
 658 time history as functions of the PGA. PGA has been increased in the range between 0.01 and  
 659 0.9 g with 0.01 g increments. Figure 18 shows the  $\delta(PGA)$  and the  $DI_{PA IDA}(\delta)$  functions  
 660 obtained. The median values and the deterministic functions are also shown in this figure.

661 Then the deterministic capacity curve has been used to determine the parameter  $\alpha$  used  
 662 to fit the Energy and Stiffness damage functions to the Park and Ang index according to the  
 663 damage model explained above. Figure 19 shows the results obtained. In this figure the Park  
 664 and Ang indices obtained are shown together with the corresponding fits. Median values of  
 665 the Park and Ang indices and of the fits are also shown. Moreover the fit of the median Park  
 666 and Ang indices and the damage model corresponding to the median  $\alpha$  value are also shown.  
 667 It can be seen that equivalent values are obtained by using the median of the fits, the fit of the  
 668 median Park and Ang indices and the damage model corresponding to the median  $\alpha$  value;

4

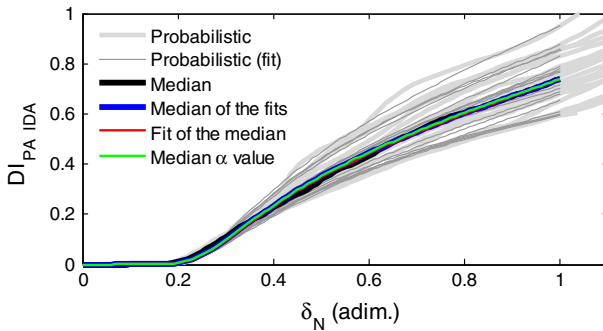


**Fig. 19** Probabilistic damage model. Median values are shown together with the results of twenty simulations and the corresponding fits of the damage model

**Table 10** Statistics of the probabilistic approach

	Median	Mean	SD	c.o.v. (%)
$m$ (kN/cm)	285.1	285.6	0.31	0.1
$T$ (s)	0.29	0.29	0.003	0.9
$\delta_u$ (cm)	8.70	8.78	1.20	13.7
$F_u$ (kN)	770.83	773.24	32.55	4.2
$\mu$	0.24	0.25	0.04	15.8
$\sigma$	0.31	0.31	0.07	21.2
$\alpha$	0.69	0.70	0.04	6.4

Median, mean, standard deviations (SD) and coefficients of variations (c.o.v.) are shown for the five parameters of the capacity curve, for the fundamental period,  $T$ , and for the parameter  $\alpha$  that defines the damage model

669 the median  $\alpha$  value is the same that the one obtained by fitting the damage model to the  
670 median of the Park and Ang damage functions, namely  $\alpha = 0.69$ .

671 Uncertainties in the  $\alpha$  parameter are slightly over 6%. Note that the damage model is  
672 also highly influenced by the normalization of the roof displacement of  $DI_{PA\ IDA}(\delta)$  function  
673 by  $\delta_u$ .

674 Table 10 summarizes the statistics of the obtained results for the capacity and damage  
675 models. The five parameters that define the capacity model are shown. The fundamental  
676 period is also included. It can be seen how the uncertainties in the initial slope,  $m$ , and indeed  
677 in the fundamental period,  $T$ , are very small, less than 1%;. Conversely the uncertainties in  
678 the ultimate base shear force,  $F_u$ , and in the ultimate roof displacement,  $\delta_u$ , are significant,  
679 mainly in  $\delta_u$  where uncertainties of about 14% are obtained. This high uncertainties are  
680 transferred to the parameters,  $\mu$  and  $\sigma$ , controlling the normalized nonlinear capacity curve.  
681 It must be reminded that the construction of the normalized nonlinear capacity curve involves  
682 the use of  $\delta_u$  and  $F_u$  in the normalization procedure. Uncertainties in the  $\alpha$  parameter are  
683 slightly over 6%. Note that the damage model is also highly influenced by the normalization  
684 of the roof displacement of  $DI_{PA\ IDA}(\delta)$  function by  $\delta_u$ .

685 These facts indicate the importance of the ultimate capacity point in the capacity and  
686 damage models here proposed. We have seen above that this ultimate capacity point is also  
687 crucial in the fragility models.

688 **7 Summary and discussion**

689 The separation of the linear and nonlinear components of the capacity curve has allowed  
690 focusing attention on the nonlinear component, which represents the progression of the  
691 degradation of the structure with increasing displacements. Because of its normalization in  
692 abscissae and ordinates, this Nonlinear Normalized Component (CNLN) is the same for  
693 capacity curves and for capacity spectra. The CNLN has been modeled by means of the  
694 cumulative integral of a cumulative lognormal function, being fully defined by two parameters  
695  $\mu$  and  $\sigma$ . The cumulative beta function with parameters  $\lambda$  and  $\nu$ , also provides excellent fits.  
696 An important property of the model is that it is infinitely differentiable and it fits well at  
697 least the first two derivatives of the CNLN. Furthermore, the CNLN is independent of the  
698 fundamental period of the building and of the ultimate capacity point, so that a specific  
699 model is representative of a large family of capacity curves/spectra. Thus, any capacity  
700 curve/spectrum is defined by five independent parameters. These parameters are, in addition  
701 to  $\mu$  and  $\sigma$ , the slope,  $m$ , of the linear part of the capacity curve, and the coordinates,  $D_u$   
702 and  $A_u$ , of the ultimate capacity point. The slope at the ultimate capacity point,  $m^*$ , can be  
703 estimated from these five parameters.

704 Concerning to expected damage, two new damage-related functions have been defined.  
705 The first one is associated to the relative variation of the secant stiffness; the second one is  
706 linked to the dissipated energy. The incremental nonlinear dynamic analysis, applied to a  
707 reinforced concrete building, has allowed observing how the Park and Ang damage index  
708 can be obtained directly by means of a linear combination of these two functions, being  
709 the contribution of the stiffness degradation about 80 losses, about 20%, for the building  
710 studied herein. However, the partition coefficient between the contributions of the stiffness  
711 and energy functions may depend on the characteristics of the seismic action. For instance, a  
712 longer duration of the earthquake may increase the contribution to the damage of the function  
713 of energy.

714 Moreover, the relationship between the Park and Ang damage index and the observations  
715 of damage pointed out by Park et al. (1985) and other authors has been used to define new  
716 damage states thresholds that, in our opinion, improve previous proposals. The acceptance  
717 of the hypothesis that the damage is distributed according a binomial distribution, allows  
718 constructing generalized fragility curves, which depend only on the parameters of the model;  
719 that is,  $\mu$  and  $\sigma$  for the lognormal function. Thus, these fragility curves are representative for  
720 a broad family of capacity curves/spectra with different initial slopes and different ultimate  
721 capacity points. However, there are two critical issues in this simple formulation of the  
722 damage model and fragility curves: (i) the definition of the ultimate capacity point; (ii) the  
723 damage states thresholds, defined as the normalized displacements where the probability of  
724 exceedance of the damage state is 0.5. Suitable values have been taken here in order to show  
725 the potentiality of the use of the CNLN in assessments of seismic damage and risk.

726 The massive use of this model has allowed focusing attention on the CNLN and establish-  
727 ing new procedures to calculate, in a simple and straightforward way, the yielding point of  
728 the bilinear capacity spectrum and the expected damage. Concerning to the yielding point, its  
729 displacement, normalized by the displacement of the ultimate capacity point, is the inverse  
730 of the ductility factor, and, can be calculated, also in a very simple manner, starting from the  
731 area under the CNLN. Thus, this normalized displacement and, consequently, also the duc-  
732 tility, can be tabulated as an empirical function of  $\mu$  and  $\sigma$ . Moreover, the bilinear capacity  
733 spectrum is a special case for  $\mu$  equal to the normalized displacement of the yielding point  
734 and  $\sigma$  null.

The method has been tested on a large number of reinforced concrete buildings with different seismic actions, always with excellent results. More work, with different building types and different seismic actions, will establish better the variability of the contributions to damage of the stiffness degradation and energy functions, as well as, it will allow a better setting of the damage states thresholds of the new generalized fragility curves. Once these thresholds are determined, as our new generalized fragility curves only depend on the CNLN, the parameters of each fragility curve may be also tabulated as functions of  $\mu$  and  $\sigma$ , likewise we have tabulated the ductility factor.

The availability of this new mathematical model for capacity curves/spectra can be a powerful tool for current earthquake engineering research. In particular, this model can be very useful in probabilistic approaches, as well as in seismic risk analyses at territorial scale since the simple modeling of the capacity curves/spectra may significantly reduce computation times.

To finish, permit us a brief digression. [Fost \(2007\)](#) quotes Frédéric Chopin: “*Simplicity is the final achievement. After one has played a vast quantity of notes and more notes, it is simplicity that emerges as the crowning reward of art*”. The phrase “*Simplicity is the ultimate sophistication*” although it appears in the novel by [Gaddis \(1955\)](#) and was used by Apple as a slogan in 1984, is attributed to Leonardo Da Vinci ([Granat 2003](#)). The Art relates to capturing beauty through simple strokes, Science to the search for simple models able to explain complex phenomena. The capacity spectrum method (CSM) achieves to pick up on the *pushover* curve, the structural response of buildings and structures of great complexity and is a shining example of this idea. The CNLN and its parametric model are also surprisingly simple but their potentiality may be significant.

**Acknowledgments** The thoughtful comments and suggestions of an anonymous reviewer helped to significantly improve the manuscript; his thorough review is highly appreciated and acknowledged. This work has been partially funded by the Spanish Government, by the European Commission and with FEDER funds, through the research projects: CGL2008-00869/BTE, CGL2011-23621, SEDUREC-CONSOLIDER-CSD2006-00060, INTERREG:POCTEFA 2007-2013/73/08, MOVE-FT7-ENV-2007-1-211590 and DESURBS-FP7-2011-261652. Y.F. Vargas-Alzate, has been the holder of a scholarship and a contract funded by the Geological Institute of Catalonia and the Polytechnic University of Catalonia by means of a bilateral agreement. Several quotes related to *simplicity* concept have been extracted from Wikipedia.

## References

- Ambraseys N, Smit P, Sigbjornsson R, Suhadolc P, Margaris B (2002) Internet-site for European strong-motion data. European Commission, Research-Directorate General, Environment and Climate Programme. [http://www.isesd.hi.is/ESD\\_Local/home.htm](http://www.isesd.hi.is/ESD_Local/home.htm). Accessed 05 May 2014
- Ambraseys N, Smit P, Douglas J, Margaris B, Sigbjornsson R, Olafsson S, Suhadolc P, Costa G (2004) Internet-site for European strong-motion data. *Boll Geofis Teor Appl* 45(3):113–129
- ATC (1985) ATC-13. Earthquake damage evaluation data for California. Applied Technology Council, Redwood City, CA
- ATC (1991) ATC-25. Seismic vulnerability and impact of disruption of lifelines in the conterminous United States. Applied Technology Council. Funded By Federal Emergency Management Agency. ATC Redwood City, CA
- ATC (1996) ATC-40. Seismic evaluation and retrofit of concrete buildings. Applied Technology Council, Redwood City, CA
- Barbat AH, Pujades LG, Lantada N, Moreno R (2006a) Performance of buildings under earthquake in Barcelona, Spain. *Comput Aided Civil Infrastruct Eng* 21:573–593
- Barbat AH, Lagomarsino S, Pujades LG (2006b) Vulnerability assessment of dwelling buildings. In: Oliveira CS, Roca A, Goula X (eds) Chapter 6: Assessing and managing earthquake risk. Springer, Dordrecht, pp 115–134

- 784 Barbat AH, Pujades LG, Lantada N, Moreno R (2008) Seismic damage evaluation in urban areas using the  
785 capacity spectrum method: application to Barcelona. *Soil Dyn Earthq Eng* 28:851–865
- 786 Barbat AH, Vargas-Alzate YF, Pujades LG, Hurtado JE (2013) Evaluación probabilista del riesgo sísmico  
787 de estructuras con base en la degradación de rigidez. *Revista Internacional de Métodos numéricos para*  
788 *cálculo y diseño en ingeniería*. Paper RIMNI-D-13-00044 (under review)
- 789 Bertero VV (1996) State of art report on design criteria. In: *Proceedings 11th world conference on earthquake*  
790 *engineering, Acapulco, Mexico, 23–28 June 1996*
- 791 Bertero VV (1997) Performance-based seismic engineering: a critical review of proposed guidelines. In:  
792 Fajfar, Krawinkler (eds) *Proceedings, seismic design methodologies for the next generation of codes,*  
793 *Bled, Slovenia, 23–27 June 1997*, pp 1–31, A. A. Balkema, Rotterdam
- 794 Bertero VV (2000) Performance-based seismic engineering: conventional vs. innovative approaches. In: *Pro-*  
795 *ceedings of the 12WCEE 2000 : 12th world conference on earthquake engineering, Auckland, New*  
796 *Zealand, paper no. 2074*, 8 pp
- 797 Bhatt C, Bento R (2011) Extension of the CSM-FEMA440 to plan-asymmetric real building structures. *Earthq*  
798 *Eng Struct Dyn* 40(11):1263–1282
- 799 Bhatt C, Bento R (2013) The extended adaptive capacity spectrum method for the seismic assessment of plan  
800 asymmetric buildings. *Earthq Spectra*. doi:10.1193/022112EQS048M
- 801 BS EN (2005) Eurocode 2: design of concrete structures—part 1–1: general rules and rules for buildings.  
802 British Standards Institution
- 803 Carr AJ (2000) Ruaumoko—inelastic dynamic analysis program. Department of Civil Engineering, University  
804 of Canterbury, Christchurch
- 805 Casarotti C, Pinho R (2007) An adaptive capacity spectrum method for assessment of bridges subjected to  
806 earthquake action. *Bull Earthq Eng* 5(3):377–390
- 807 CEN (2004) Eurocode 8: Design of structures for earthquake resistance. Part 1: general rules, seismic actions  
808 and rules for buildings. EN 1998–1:2004. Comité Européen de Normalisation, Brussels
- 809 Chopra AK, Goel RK (1999) Capacity-demand-diagram methods based on inelastic design spectrum. *Earthq*  
810 *Spectra* 15(4):637–656
- 811 Chopra AK, Goel RK (2004) A modal pushover analysis procedure to estimate seismic demand for  
812 unsymmetric-plan buildings. *Earthq Eng Struct Dyn* 33(8):903–927
- 813 Cosenza E, Manfredi G (2000) Damage indices and damage measures. *Prog Struct Mat Eng* 2(1):50–59
- 814 Fajfar P (1999) Capacity spectrum method based on inelastic demand spectra. *Earthq Eng Struct Dyn* 28:979–  
815 993
- 816 Fajfar P, Gaspersic P (1996) The N2 method for the seismic damage analysis of RC buildings. *Earthq Eng*  
817 *Struct Dyn* 25(1):31–46
- 818 Fajfar P, Marušić D, Perus I (2005a) The extension of the N2 method to asymmetric buildings. In: *Proceedings*  
819 *of the 4th European workshop on the seismic behavior of irregular and complex structures, Thessaloniki*
- 820 Fajfar P, Marusic D, Perus I (2005b) Torsional effects in the pushover-based seismic analysis of buildings.  
821 *J Earthq Eng* 9(6):831–854
- 822 FEMA (2002) Earthquake loss estimation methodology. HAZUS'99 (SR 2) technical manual. Federal Emergency  
823 Management Agency, Washington, DC
- 824 Fost J (2007) *If not God, Then What?* Clearhead Studios, Inc. 288 pp
- 825 Freeman SA (1998a) Development and use of capacity spectrum method. In: *Proceedings of 6th U.S. national*  
826 *conference of earthquake engineering*. EERI, Seattle
- 827 Freeman SA (1998b) The capacity spectrum method as a tool for seismic design. In: *Proceedings of the*  
828 *eleventh European conference on earthquake engineering, Paris, 1998*
- 829 Freeman SA (2004) Review of the development of the capacity spectrum method, paper No. 438. *J Earthq*  
830 *Technol* 41(1): 1–13
- 831 Freeman SA, Nicoletti JP, Tyrell JV (1975) Evaluations of existing buildings for seismic risk—a case study of  
832 Puget Sound Naval Shipyard, Bremerton, Washington. In: *Proceedings of 1st U.S. national conference*  
833 *of earthquake engineering*. EERI, Berkeley, pp 113–122
- 834 Gaddis W (1955) *The Recognitions*. Dalkey Archive Press, February 7, 2012, 976 pp
- 835 Gencturk B, Elnashai AS (2008) Development and application of an advanced capacity spectrum method. *Eng*  
836 *Struct* 30:3345–3354
- 837 Giovinazzi S (2005) The vulnerability assessment and the damage scenario in seismic risk analysis. Ph.D  
838 dissertation. University of Florence (I) and Technical University of Braunschweig (D). [http://digisrv-1.](http://digisrv-1.biblio.etc.tu-bs.de:8080/docportal/receive/DocPortal_document_00001757)  
839 [biblio.etc.tu-bs.de:8080/docportal/receive/DocPortal\\_document\\_00001757](http://digisrv-1.biblio.etc.tu-bs.de:8080/docportal/receive/DocPortal_document_00001757). Accessed on 07 Jan 2014
- 840 Granat H (2003) *Wisdom through the ages: book two*. Miklen Press, Poulsbo, Washington, 300 pp
- 841 Grünthal G (1998) *European Macroseismic Scale*. Centre Européen de Géodynamique et de Séismologie,  
842 Luxembourg, vol 15

- 843 Lagomarsino S, Giovinazzi S (2006) Macroseismic and mechanical models for the vulnerability and damage  
 844 assessment of current buildings. *Bull Earthq Eng* 4(4):415–443
- 845 Lantada N, Pujades LG, Barbat AH (2009) Vulnerability index and capacity spectrum based methods for urban  
 846 seismic risk evaluation: a comparison. *Nat Hazards* 51:501–524
- 847 Lantada N, Irizarry J, Barbat AH, Goula X, Roca A, Susagna T, Pujades LG (2010) Seismic Hazard and  
 848 risk scenarios for Barcelona, Spain, using the Risk-UE vulnerability index method. *Bull Earthq Eng*  
 849 8(2):201–229
- 850 Limpert E, Stahel WA, ABBT M (2001) Log-normal distributions across the sciences: keys and clues. *Bio-*  
 851 *Science* 51(5):341–352
- 852 Milutinovic ZV, Trendafiloski GS (2003) WP04 Vulnerability of current buildings RISK-UE project of the  
 853 EC: an advanced approach to earthquake risk scenarios with applications to different European towns
- 854 Otani S (1974) Inelastic analysis of RC frame structures. *J Struct Div ASCE* 100(7):1433–1449
- 855 Park YJ (1984) Seismic damage analysis and damage-limiting design of R/C structures. PhD Thesis, Depart-  
 856 ment of Civil Engineering, University of Illinois, Urbana, IL
- 857 Park YJ, Ang AH-S (1985) Mechanistic seismic damage model for reinforced concrete. *J Struct Eng ASCE*  
 858 111(4):722–739
- 859 Park YJ, Ang AH-S, Wen YK (1985) Seismic damage analysis of reinforced concrete buildings. *J Struct Eng*  
 860 111:740–757
- 861 Park YJ, Ang AH-S, Wen YK (1987) Damage-limiting aseismic design of buildings. *Earthq Spectra* 3(1):1–26  
 862
- 863 Pinho R, Marques M, Monteiro R, Casarotti, C (2008) Using the adaptive capacity spectrum method for  
 864 seismic assessment of irregular frames. In: *Proceedings of the 5th European workshop on the seismic*  
 865 *behaviour of irregular and complex structures*, Catania, Italy
- 866 Pinho R, Monteiro R, Casarotti C, Delgado R (2009) Assessment of continuous span bridges through nonlinear  
 867 static procedures. *Earthq Spectra* 25(1):143–159
- 868 Pujades LG, Barbat AH, González-Drigo JR, Avila J, Lagomarsino S (2012) Seismic performance of a block  
 869 of buildings representative of the typical construction in the example district in Barcelona (Spain). *Bull*  
 870 *Earthq Eng* 10:331–349
- 871 Sawyer HA Jr (1964) Status and potentialities of nonlinear design of concrete frames. In: *Proceedings, interna-*  
 872 *tional symposium on flexural mechanics of reinforced concrete*, Miami, Florida, 10–12 November 1964,  
 873 *ASCE 1965 50 and ACI SP 12*, pp 7–28
- 874 SEAOC (1995) Vision 2000 Committee. Performance based seismic engineering of buildings. *Structural*  
 875 *Engineers Association of California (SEAOC)*, Sacramento, USA, report, 1995, 115 pp
- 876 Vamvatsikos D, Cornell CA (2001) The incremental dynamic analysis. *Earthq Eng Struct Dyn* 31(3):491–514
- 877 Vargas-Alzate YF (2013) Análisis estructural estático y dinámico probabilista de edificios de hormigón armado.  
 878 Aspectos metodológicos y aplicaciones a la evaluación del daño. PhD Thesis. Universidad Politécnica  
 879 de Cataluña, BarcelonaTech. Barcelona, 203 pp
- 880 Vargas-Alzate YF, Pujades LG, Barbat AH, Hurtado JE (2013a) Incremental dynamic analysis and pushover  
 881 analysis of buildings. A probabilistic comparison. *Computational methods in stochastic dynamics*, vol  
 882 2. Springer, pp 293–308
- 883 Vargas-Alzate YF, Pujades LG, Barbat AH, Hurtado JE (2013b) Capacity, fragility and damage in reinforced  
 884 concrete buildings: a probabilistic approach. *Bull Earthq Eng* 11:2007–2032
- 885 Vargas-Alzate YF, Barbat AH, Pujades LG, Hurtado JE (2013c) Probabilistic seismic risk evaluation of RC  
 886 buildings. In: *Proceedings of the ICE—structures and buildings*. Available online 10 September 2013.  
 887 2012. doi:10.1680/stbu.12.00031
- 888 Vargas-Alzate YF, Pujades LG, Barbat AH, Hurtado JE (2013d) Evaluación probabilista de la capacidad,  
 889 fragilidad y daño sísmico en edificios de hormigón armado. *Revista Internacional de Métodos Numéricos*  
 890 *para Cálculo y Diseño en Ingeniería* 29(2):63–78
- 891 Williamson EB (2003) Evaluation of damage and P- $\Delta$  effects for systems under earthquake excitation. *J Struct*  
 892 *Eng ASCE* 129(3):1036–1046
- 893 Williamson EB, Kaewkulchai G (2004) Computational modeling of structural collapse. In: *The fifth U.S.–Japan*  
 894 *workshop on performance-based earthquake engineering methodology for reinforced concrete building*  
 895 *structures*. 10–11 September 2003. PEER report 2003/11. Pacific Earthquake Engineering Research  
 896 Center. College of Engineering. University of California, Berkeley. February 2004, pp 225–238